



# Gallic acid induces T-helper-1-like T<sub>reg</sub> cells and strengthens immune checkpoint blockade efficacy

Biaolong Deng,<sup>1</sup> Biaolong Yang,<sup>2</sup> Jieqiong Chen,<sup>3</sup> Shuaiwei Wang,<sup>1</sup> Weiqi Zhang,<sup>1</sup> Yixian Guo <sup>4</sup>, Yichao Han,<sup>5</sup> Hecheng Li,<sup>5</sup> Yongjun Dang,<sup>6</sup> Yaqin Yuan,<sup>1</sup> Xueyu Dai,<sup>1</sup> Yuansheng Zang,<sup>2</sup> Yangyang Li <sup>7</sup>, Bin Li<sup>1,8,9,10,11</sup>

**To cite:** Deng B, Yang B, Chen J, *et al.* Gallic acid induces T-helper-1-like T<sub>reg</sub> cells and strengthens immune checkpoint blockade efficacy. *Journal for ImmunoTherapy of Cancer* 2022;**10**:e004037. doi:10.1136/jitc-2021-004037

► Additional supplemental material is published online only. To view, please visit the journal online (<http://dx.doi.org/10.1136/jitc-2021-004037>).

BD and BY contributed equally.

Accepted 09 June 2022



© Author(s) (or their employer(s)) 2022. Re-use permitted under CC BY-NC. No commercial re-use. See rights and permissions. Published by BMJ.

For numbered affiliations see end of article.

## Correspondence to

Professor Bin Li;  
binli@shsmu.edu.cn

Dr Yuansheng Zang;  
doctorzangys@163.com

Dr Yangyang Li;  
yangyangli@shanghaitech.edu.cn

## ABSTRACT

**Background** Foxp3<sup>+</sup> regulatory T (T<sub>reg</sub>) cells facilitate tumor immune evasion by forming a suppressive tumor microenvironment. Therefore, immune therapies promoting T<sub>reg</sub> fragility may greatly enhance immune checkpoint blockade (ICB) efficacy in cancers.

**Methods** We have screened 2640 compounds and identified the gut microbial metabolite gallic acid, which promotes Foxp3 degradation and T<sub>reg</sub> instability by repressing *Usp21* gene transcription. In vivo and in vitro experiments have been performed to explore the roles of *Usp21* in T<sub>reg</sub> cells. Importantly, we treated tumor-bearing mice with gallic acid and anti-PD-1 antibody to explore the potential therapeutic value of gallic acid in clinical cancer immunotherapy.

**Results** Mechanistically, gallic acid prevents STAT3 phosphorylation and the binding of phosphorylated STAT3 to *Usp21* gene promoter. The deubiquitinated *Usp21* and stabilized PD-L1 proteins boost the function of T<sub>reg</sub> cells. Combination of gallic acid and anti-PD-1 antibody, in colorectal cancer (CRC) treatment, not only significantly dampen T<sub>reg</sub> cell function by impairing PD-L1/PD-1 signaling and downregulating Foxp3 stability, but also promote CD8<sup>+</sup> T cells' production of IFN-γ and limited tumor growth.

**Conclusion** Our findings have implications for improving the efficacy of ICB therapy in CRC by inducing T-helper-1-like Foxp3<sup>lo</sup> T<sub>reg</sub> cells.

## INTRODUCTION

During cancer development, cytotoxic T lymphocytes (CTLs) progressively differentiate into a dysfunctional and exhausted state marked by the accumulation of surface inhibitory receptors and reduction in effector functions.<sup>1</sup> CD8<sup>+</sup> T cells provide immunity against cancer by recognizing 'foreign-looking' antigens presented on the surface of cancerous cells.<sup>2</sup> However, when infection persists for a long period, CD8<sup>+</sup> T cells adapt to this stress by desensitizing their T cell antigen receptor (TCR) via the upregulation of inhibitory receptors such as PD-1, TIM-3, LAG-3 and TIGIT, which prevents T cells deterioration caused by overstimulation. This coping

## WHAT IS ALREADY KNOWN ON THIS TOPIC

⇒ We knew that T<sub>reg</sub> cells played a vital role in tumor immune evasion. Therefore, immune therapies modifying T<sub>reg</sub> plasticity may greatly enhance immune checkpoint blockade (ICB) efficacy in cancers.

## WHAT THIS STUDY ADDS

⇒ We revealed that gallic acid inhibits *Usp21* expression by decreasing STAT3 phosphorylation, further dampens FOXP3 and PD-L1 stability and modulates T<sub>reg</sub> cells functions. We elucidated the mechanisms for gallic acid to repress colorectal cancer (CRC) development and strengthen anti-PD-1 blockade efficacy.

## HOW THIS STUDY MIGHT AFFECT RESEARCH, PRACTICE OR POLICY

⇒ Our findings provide a new strategy to improve the efficacy of ICB therapy in CRC treatment by inducing Th1-like PD-L1<sup>lo</sup>Foxp3<sup>lo</sup> T<sub>reg</sub> cells.

mechanism also reduces the ability of CD8<sup>+</sup> T cells to kill tumor cells, produce inflammatory cytokines (such as IFN-γ and TNF), and proliferate and form long-term memory cells.<sup>3</sup> Recently, several groups have reported that the nuclear factor TOX (thymocyte selection-associated HMG BOX) as the key factor which mediates transcriptional and epigenetic changes, which are critical for the adaptation of CD8<sup>+</sup> T cells to chronic stress.

Recent immune checkpoint blockade (ICB) of PD-1 enhances immune surveillance by reinvigorating exhausted PD-1<sup>+</sup> CTLs to kill tumor cells, which has shown clinical efficacy in a variety of cancer types and even in patients with advanced stages of cancer.<sup>4–6</sup> However, only a subset (15%–30%) of patients exhibit durable antitumor immune responses after anti-PD-1 treatment, suggesting the requirement of therapeutic strategies (eg, targeting protumorigenic or immune suppressive cells) to potentiate antitumor immunity.<sup>7–11</sup> More importantly, in about 10% of patients with

advanced gastric cancer, PD-1 blockade promotes hyperprogression of cancer by facilitating the amplification of PD-1 +regulatory T ( $T_{reg}$ ) cells.<sup>12</sup> Overall, immunotherapy has greatly revolutionized the therapeutic interventions in cancer treatments, but its efficacy remains quite limited in clinical settings.

$T_{reg}$  cells express the key transcription factor Foxp3 and critically maintain immune tolerance in tumor microenvironment (TME) by suppressing antitumor immunity.<sup>11,13,14</sup> For instance, tumor infiltrating  $T_{reg}$  cells, with upregulated PD-L1 expression, significantly suppress exhausted PD-1<sup>+</sup> cytotoxic T cells.<sup>15,16</sup> In addition, neuropilin-1 (Nrp1) also strengthens the function of intra-tumoral  $T_{reg}$  cells.<sup>17</sup> Mechanistically, Nrp1-deficient  $T_{reg}$  cells produce interferon- $\gamma$  (IFN- $\gamma$ ), which drives the fragility of surrounding wild-type (WT)  $T_{reg}$  cells in the TME, thus, boosts antitumor immune responses and significantly improves the efficacy of PD-1 blockade therapy.<sup>18</sup> Therefore, immune therapies that directly promote  $T_{reg}$  cell fragility may greatly improve the efficacy of ICB efficacy in cancer treatment.

The significant challenge of targeting  $T_{reg}$  cells is to specifically modulate their stability and plasticity in TME. Instability of  $T_{reg}$  cells, characterized by polyubiquitination-mediated degradation of Foxp3 and acquisition of pro-inflammatory T-helper-1 (Th1)-like properties, facilitates effective antitumor immunity.<sup>19–25</sup> By contrast,  $T_{reg}$  cells with the suppressive MondoA-TXNIP axis promote glycolysis and display a Th17-like phenotype, leading to interleukin-17A (IL-17A) prominent microenvironment, CD8<sup>+</sup> T-cell exhaustion and colorectal carcinogenesis.<sup>26</sup> For these reasons, specific induction of Th1-like Foxp3<sup>lo</sup>  $T_{reg}$  cells may restrain tumor progression by making ICB safer and more effective for cancer immunotherapies.

Tissue-resident  $T_{reg}$  cells lacking Usp21 are instable, which confer a Th1-like Foxp3<sup>lo</sup> phenotype and may further promote antitumor immune responses.<sup>21</sup> In colorectal cancer (CRC), Foxp3<sup>lo</sup>  $T_{reg}$  cells are less immune suppressive, produce IFN- $\gamma$  and are consistent with better prognosis.<sup>8</sup> Conceivably, induction of Th1-like Foxp3<sup>lo</sup>  $T_{reg}$  cells by targeting Usp21, rather than depletion of total  $T_{reg}$  cells, may greatly increase ICB efficacy and prevent colorectal carcinogenesis, but research on this topic has been quite limited.

We have screened 2640 compounds and identified gallic acid, which promotes Foxp3 degradation by suppressing Usp21 gene transcription, leading to the generation of Th1-like Foxp3<sup>lo</sup>  $T_{reg}$  cells. Mechanistically, gallic acid inhibits STAT3 phosphorylation and prevents the binding of phosphorylated STAT3 (p-STAT3) to the promoter of *Usp21* gene. We further reveal that Usp21 additionally deubiquitinates and stabilizes PD-L1 to strengthen  $T_{reg}$  cell function. A combined immunotherapy against CRC, using gallic acid and anti-PD-1 antibody simultaneously, significantly dampens Treg cell function by impairing PD-L1/PD-1 signaling and Foxp3 stability as well as promotes cytotoxic T cells' expression of IFN- $\gamma$ , thus, limits tumor growth. Our findings provide a new strategy

to improve the efficacy of ICB therapy in CRC treatment by inducing Th1-like Foxp3<sup>lo</sup>  $T_{reg}$  cells.

## METHODS

### Mice

In this study, all mouse lines were maintained on a C57BL/6J background. *Foxp3*<sup>Cre</sup> mice were purchased from the Jackson Laboratory (stock number: 016959, Bar Harbor, USA). *Usp21*<sup>fl/fl</sup> mice were described in previous report.<sup>21</sup> To exclude cage effects, heterozygotes (For example, *Usp21*<sup>fl/+</sup>*Foxp3*<sup>Cre</sup> $\times$ *Usp21*<sup>fl/+</sup>*Foxp3*<sup>Cre</sup>) were bred to generate Treg-specific KO mice, *Usp21*<sup>fl/fl</sup>*Foxp3*<sup>Cre</sup> and *Foxp3*<sup>Cre</sup> (control) mice. *Foxp3*<sup>Cre</sup> (WT) and *Usp21*<sup>fl/fl</sup>*Foxp3*<sup>Cre</sup> (KO) mice of C57BL/6 strain were maintained in the animal facility of Shanghai Jiao Tong University School of Medicine under specific pathogen-free conditions. Animal experiments were conducted in accordance with institutional guidelines approved by the Institutional Animal Care and Use Committee Shanghai Jiao Tong University School of Medicine.

### Cell lines

The C57BL/6 murine colon MC38 adenocarcinoma cell line were routinely cultured at 37°C and 5% CO<sub>2</sub> in Dulbecco's modified eagle medium (DMEM) supplemented with 10% fetal bovine serum (FBS), Gibco, ThermoFisher Scientific, Waltham, MA, USA), 1% penicillin, 1% streptomycin and 2mM glutamine. Human LOVO cells were purchased from the American Type Culture Collection (ATCC, Manassas, VA, USA), which were cultured at 37°C and 5% CO<sub>2</sub> in DMEM supplemented with 10% FBS, 1% penicillin, 1% streptomycin and 2mM glutamine. HEK 293T (ATCC, CRL-11268) cells were cultured at 37°C and 5% CO<sub>2</sub> in DMEM supplemented with 10% FBS, 1% penicillin, 1% streptomycin and 2mM glutamine. Cell lines were tested for mycoplasma contamination before use.

### TCGA data analysis

Survival analysis, using TCGA COAD data, was performed to evaluate the association of individual gene or gene sets derived from specific cell clusters with GC prognosis. The statistical analysis of gene expression and the clinical outcomes were performed by GEPIA2 and Kaplan-Meier plotter.<sup>27,28</sup> The mean expression of given signatures was grouped into high and low expression groups by the 25 th and 75 th quantile values.

### Human CRC patients' specimens

Blood, paratumor and tumor samples from CRC patients were obtained from the Department of Gastrointestinal Surgery, Renji Hospital, Shanghai Jiao Tong University School of Medicine. The clinical criteria for patient recruitment were as follows: (1) patients had no autoimmune disorders or other primary malignant tumors; (2) patients had not been treated with chemotherapy, radiation, or any other antitumor medicine prior to tumor

resection; (3) patients had completed clinical information, postoperative pathological diagnoses, and follow-up data. Clinical characteristic of CRC patients can be found in online supplemental table 1. Clinical characteristics of CRC patients can be found in online supplemental table 1. Tumor and paratumor tissues were excised and digested with 2 mg/mL Collagenase D (Sigma-Aldrich, St. Louis, USA Cat#11088882001) and 150 µg/mL DNase I (Sigma-Aldrich, Cat# DN25) at 37°C with shaking at 200 r.p.m for 1 hour. Lymphocytes were further analyzed by flow cytometry (described in detail below).

### Tumor engraftment

Mice were subcutaneously injected with  $2 \times 10^5$  MC38 colorectal adenocarcinoma cells or B16 melanoma cells or 4T1 mammary carcinoma cells. When palpable tumors were presented, treatment was started as described below and tumor volume was assessed by caliper measurement. Mice were sacrificed when tumor volume reached 1500 mm<sup>3</sup>. Gallic acid (5 mg/kg, Sigma-Aldrich, Cat#149-91-7), was dissolved in PBS and intraperitoneally injected daily starting on day 7. Starting on day 10, anti-PD-1 antibody (100 µg/injection, BioXCell, New Hampshire, USA, Cat#BE0146) or isotype control (100 µg/injection, BioXCell, Cat#BE0083) were intraperitoneally injected once every 3 days for three times. Mice were next transcatheterially perfused with heparin (10 U/mL, Sigma-Aldrich, Cat#H3149-25KU) in PBS under anesthesia. Tumors were collected and processed for flow cytometry. In subcutaneous tumor models, fresh tumor tissues were washed three times with RPMI 1640 before cut into small pieces. The specimens were then collected in RPMI 1640 containing 2 mg/mL collagenase D (Roche, Cat#11088882001) and 150 µg/mL DNase I (Sigma-Aldrich, Cat# DN25). The specimens were then mechanically dissociated using the gentle MACS Dissociator (Miltenyi Biotec, Bergisch Gladbach, GER). Dissociated cell suspensions were further incubated for 30 mins at 37°C under continuous rotation and filtered through 70 µm cell strainers to obtain cell suspensions. Lymphocytes were further analyzed by flow cytometry.

### Azoxymethane-dextran sodium sulfate-induced colorectal carcinogenesis mice model

Eight-week-old female mice were intraperitoneally injected with azoxymethane (AOM, 10 mg/kg, Sigma-Aldrich, Cat# A5486). Seven days later, 2% dextran sodium sulfate (DSS, 36-50 kDa, MP Biomedicals, Irvine, USA Cat# 160110) was added to drinking water for 7 days followed by regular drinking water for 2 weeks. This cycle of DSS treatment was repeated twice and mice were euthanized on day 100 after treatment. In the antibody therapy, *Foxp3*<sup>Cre</sup> and *Usp21*<sup>fl/fl</sup>*Foxp3*<sup>Cre</sup> mice were co-housed in the same cage and AOM-DSS were used to induce tumors. Anti-PD-1 (100 µg/injection, BioXCell, Cat# BE0146) or isotype control (100 µg/injection, BioXCell, Cat# BE0083,) antibodies were intraperitoneally injected once every 3 days for five times, starting on day 80. Gallic acid

(5 mg/kg, Sigma-Aldrich, Cat#149-91-7) was dissolved in PBS and injected daily starting at the 80th day. To obtain lamina propria lymphocytes, colons were opened longitudinally; washed with Hank's balanced salt solution; shaken in Hank's balanced salt solution containing 2 mmol/L EDTA at 37°C to remove epithelial cells, and incubated with collagenase VIII (Sigma-Aldrich, Cat#C5138) and deoxyribonuclease I (Sigma-Aldrich, Cat#DN25) for 40 mins. The supernatants were passed through 70 µm cell strainers. Lymphocytes were further separated by centrifugation with 40%–70% Percoll (GE Healthcare, Chicago, USA, Cat#17-0891-01) gradient and then subjected to flow cytometric analysis.

### Reagents and antibodies

The following reagents and antibodies were used in this study:

MG132 (Sigma-Aldrich, Cat#M7449); anti-Flag (Sigma-Aldrich, Cat#F7425); anti-MYC (Sigma-Aldrich, Cat#M4439); anti-STAT3 (Cell Signaling Technology, Cat#9319S); anti-phospho-STAT3 (Cell Signaling Technology, Cat#9145S).

Mouse IgG Isotype control (Cell Signaling Technology, Cat#53484).

Rabbit IgG Isotype control (Cell Signaling Technology, Cat#2729); anti-Usp21 (Invitrogen, Cat#PA5-110556); anti-beta actin (2D4H5) (Proteintech, Cat#66009-1-Ig).

### Immunoprecipitation and immunoblot analysis

HEK293T cells were transfected with indicated vectors and further lysed in 300 µL RIPA lysis buffer (50 mM Tris-HCl, pH 7.4, 150 mM NaCl, 1 mM EDTA, 5 mM EGTA, 1% Nonidet P-40, 0.25% sodium deoxycholate, 10 µg/mL aprotinin, 10 µg/mL leupeptin, and 1 mM phenylmethylsulfonyl fluoride) supplemented with protease inhibitor cocktail (1:100, Sigma-Aldrich, Cat#P8340), 1 mM NaF, and 1 mM phenylmethylsulfonyl fluoride (PMSF). For immunoprecipitation, cell lysates were cleared by centrifugation and supernatants were immunoprecipitated with the appropriate antibodies using protein A/G-agarose beads at 4°C. After washing, sample-loading buffer was added to the precipitates. Samples were then used for immunoblot analysis.

### Flow cytometry

To determine cytokine expression, cells were stimulated with 50 ng/mL phorbol 12-myristate 13-acetate (Sigma-Aldrich, Cat#P1585), 1 mM ionomycin (Sigma-Aldrich, Cat#I3909), Golgi Stop and Golgi Plug (BD Bioscience, New Jersey, USA, Cat 554724) for 4 hours. At the end of stimulation, cells were stained with fixable viability dye eFluor 780 (eBioscience, San Diego, USA, Cat#65-0865-14). For the analysis of surface markers, cells were stained in PBS containing 2% FBS (Gibco, Cat#10-082-147) with antibodies as indicated. Foxp3 staining was performed according to the manufacturer's instructions (Transcription Factor Staining Buffer Set, eBioscience, Cat#00-5523-00). For flow cytometry staining, unless

otherwise described, all antibodies were used at the final dilution of 1:200. The following antibodies were used in this study: anti-mouse CD4-PerCP-Cy5.5 (eBioscience, Cat# 45-4321-80), Anti-mouse CD8 $\alpha$ -PE-Cy7 (eBioscience, Cat# 100714), Anti-mouse IFN $\gamma$ -APC (eBioscience, Cat# 25-4015-82), Anti-mouse Foxp3-FITC (eBioscience, Cat# 71-5775-40), Anti-mouse PD-L1-BV421 (BD bioscience Cat# 564716), Anti-mouse PD-1-PE (eBioscience, Cat# 12-9981-81), Anti-human CD4-PerCP-Cy5.5 (eBioscience, Cat# 45-0048-42), Anti-human Foxp3-APC (eBioscience, Cat# 77-5774-40), Anti-human Foxp3-PE (eBioscience, Cat# 72-5774-40), Anti-human IFN- $\gamma$ -APC (eBioscience, Cat# MHCIFG05), Anti-human IFN- $\gamma$ -PE-Cy7 (eBioscience, Cat# 25-7319-41), anti-CD62L-APC (Biolegend, Cat#104412), anti-CD44-PE (Miltenyi Biotec, Bergisch Gladbach, Germany, Cat#130-118-566). All samples were acquired with an LSRFortessa X-20 cell analyzer (BD Bioscience) and analyzed with FlowJo software (TreeStar).

### In vitro expansion of human regulatory T cells

Human PBMCs were obtained from blood samples of healthy donors (Shanghai Blood Center) with ethical approval from Shanghai Blood Center Ethics Committee. Human CD4<sup>+</sup>CD25<sup>low</sup>CD127<sup>high</sup>CD45RA<sup>+</sup> naïve CD4<sup>+</sup> T cells were sorted by BD FACS Aria II cell sorter and differentiated into inducible T<sub>reg</sub> cells in X-VIVO (Lonza, Walkersville, USA, Cat#04-418Q) medium supplemented with 10% fetal bovine serum (Invitrogen, Maltham, USA, Cat#10100147), 1% GlutaMAX, 1% sodium pyruvate, 1% minimum essential medium with nonessential amino acids, 1% penicillin-streptomycin, 100 U/mL IL2 (R&D systems, Minneapolis, USA, Cat#202-IL), and 5 ng/mL transforming growth factor- $\beta$  (R&D Systems, Cat#240-B), in the presence of Dynabeads Human T-activator CD3/CD28 (Gibco, Cat#11132D) at a bead-to-cell ratio of 1:4. Approximately 7 days later, the differentiation efficiency reached at least 90% and could be used for analysis.

### In vitro suppressive assay

Human effective CD4<sup>+</sup>CD25<sup>low</sup> T cells were labeled with CellTrace Violet and sorted by BD FACS Aria II cell sorter. The labeled Teffs were then cultured alone or mixed, at different ratios, with inducible T<sub>reg</sub> cells. For T<sub>reg</sub> suppression assay, inducible T<sub>reg</sub> cells were first cultured in the presence or absence of 10  $\mu$ mol/L gallic acid for 24 hours. The treated T<sub>reg</sub> cells were then cultured with CellTrace Violet-labeled responder T cells in the presence of anti-CD3/CD28 beads for 3 days.

### His-ubiquitin pulldown assay

For ubiquitination assay, HEK293T cells were transfected with the indicated plasmids and were treated with 10  $\mu$ M MG132 for 6 hours before harvesting. Cells were lysed in a pH 8 urea buffer (8 M urea, 100 mM Na<sub>2</sub>HPO<sub>4</sub>, 10 mM TRIS (pH 8.0), 0.2% TX-100, 10 mM imidazole and 1 mM N-ethylmaleimide) and incubated with Ni-NTA beads for 2 hours at room temperature. The beads were washed twice in pH 8 urea buffer; twice in pH 6.3 urea buffer

(8 M urea, 100 mM Na<sub>2</sub>HPO<sub>4</sub>, 10 mM TRIS (pH 6.3), 0.2% TX-100 and 10 mM imidazole); and once in wash buffer (20 mM TRIS (pH 8.0), 100 mM NaCl, 20% glycerol, 1 mM dithiothreitol and 10 mM imidazole). Samples were then used for immunoblotting analysis with indicated antibodies.

### ChIP assay

Briefly,  $1 \times 10^7$  T<sub>reg</sub> cells were cross-linked with formaldehyde and the chromatin was sonicated into ~500 bp fragments. After sonication, the chromatin solution (approximately 500  $\mu$ g) was incubated with ChIP-grade antibodies against p-STAT3 (Tyr705, D3H7, CST) and rabbit IgG overnight at 4°C. The antibody-bound complexes were precipitated, and the DNA fragments extricated from these complexes were purified using a QIAquick PCR Purification Kit (Qiagen, Dusseldorf, Germany). Preimmunoprecipitated input DNA was used as control in each reaction. The purified ChIP DNA samples were analyzed by quantitative real-time PCR (qRT-PCR) with primers listed in online supplemental table 2.

### RNA extraction and qRT-PCR

Total RNA was prepared using Trizol reagent (Invitrogen) following the manufacturer's instructions. cDNA was synthesized using a reverse transcriptase kit (TaKaRa, Japan), followed by qRT-PCR analysis (SYBR Green; TaKaRa) with primers listed in online supplemental table 3).

### Statistical analysis

All data were represented as mean $\pm$ SD. Unless stated otherwise, p values were calculated with unpaired two-tailed Student's t-test in GraphPad Prism V.7.0. One-way analysis of variance (ANOVA) and two-way ANOVA were used for multiple comparisons. P values were denoted in figures in the following way: ns: not significant; \* $p < 0.05$ ; \*\* $p < 0.01$ ; \*\*\* $p < 0.001$ ; \*\*\*\* $p < 0.0001$ .

## RESULTS

### Gallic acid induces Th1-like FOXP3<sup>lo</sup> T<sub>reg</sub> cells

To induce Th1-like FOXP3<sup>lo</sup> T<sub>reg</sub> cells, might prevent colorectal carcinogenesis, we first screened 2640 compounds and identified 31 small molecules that could downregulate the protein levels of FOXP3, including the gut microbial metabolite gallic acid<sup>29</sup> (figure 1A). Flow cytometric analysis further confirmed that gallic acid treatment induced the decrease of FOXP3 protein expression (figure 1B,C) and simultaneously production of IFN- $\gamma$  (figure 1D,E). Interestingly, *Foxp3* gene was still actively transcribed after gallic acid treatment (figure 1F), suggesting that gallic acid compromised the stability of FOXP3 protein potentially through post-translational modification.

To investigate how gallic acid modulated FOXP3 protein stability, we next examined the expression of verified E3 ubiquitin ligases and deubiquitinases of FOXP3 in

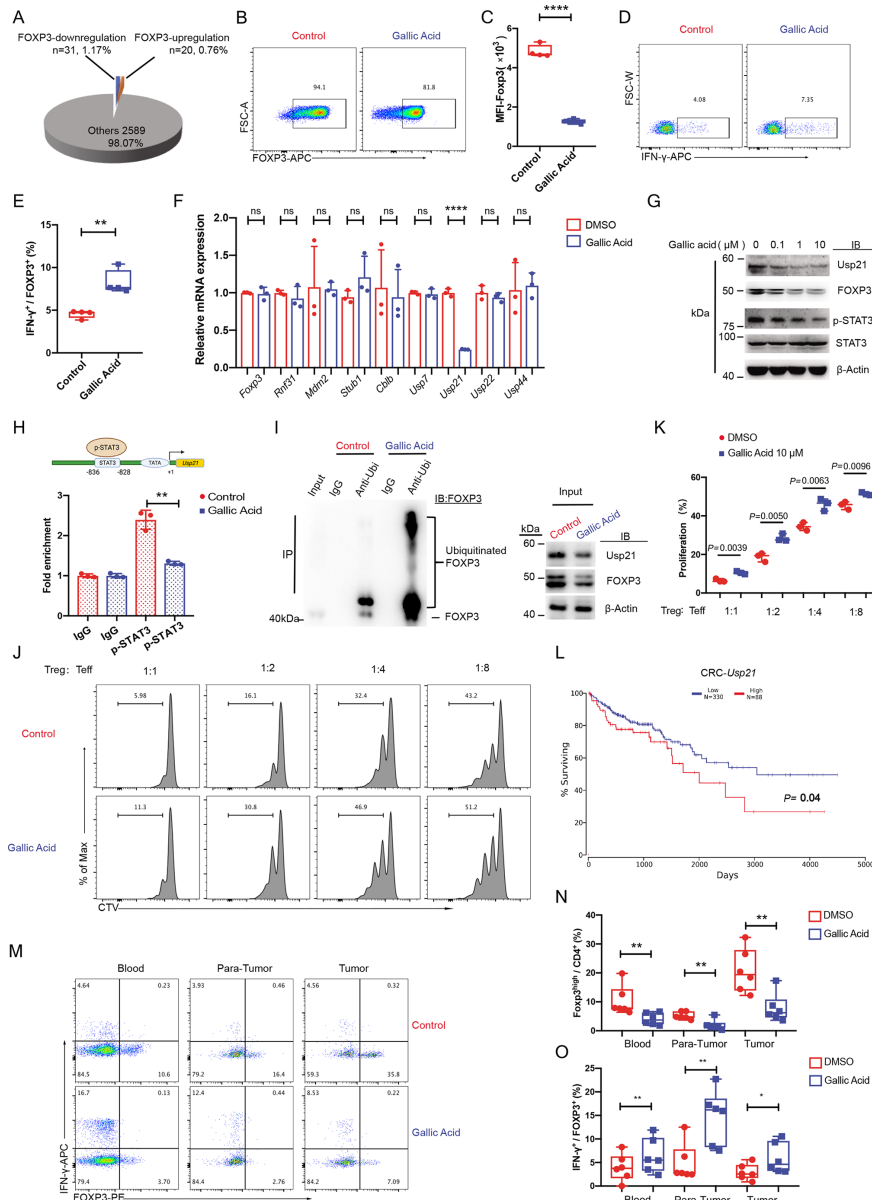


**Figure 1** Gallic acid induces Th1-like  $T_{reg}$  cells by suppressing *Usp21* gene transcription. (A) Human  $iT_{reg}$  cells were polarized from naïve  $CD4^+$  T cells and further treated with small molecules ( $n=2640$ ) for 48 hours. FOXP3 levels were next analyzed by flow cytometry. (B) Representative figure show the expression of FOXP3 protein in  $iT_{reg}$  cells treated with or without gallic acid ( $10\mu M$ ) for 48 hours ( $n=4$  per group). (C) Mean fluorescent intensity (MFI) of FOXP3 in  $iT_{reg}$  cells as indicated in (B). (D) Representative figure shown the expression of IFN- $\gamma$  in FOXP3 $^+$   $iT_{reg}$  cells treated with or without gallic acid ( $10\mu M$ ) for 48 hours ( $n=4$  per group). (E) Percentages of IFN- $\gamma^+$ FOXP3 $^+$   $iT_{reg}$  cells as indicated in (D). (F) Relative expressions levels of *Foxp3*, *Rnf31*, *Mdm2*, *Stub1*, *Cblb*, *Usp7*, *Usp21*, *Usp22* and *Usp44* mRNAs in  $iT_{reg}$  cells treated with or without gallic acid ( $10\mu M$ ) for 48 hours ( $n=3$  per group). (G) Representative Western blot shown the expression of USP21, FOXP3, phosphorylated STAT3 (p-STAT3) and total STAT3 proteins in  $iT_{reg}$  cells treated with indicated doses of gallic acid for 48 hours. (H) ChIP-qPCR analysis of p-STAT3 occupancy on the promoter of *Usp21* gene in human  $iT_{reg}$  cells treated with or without gallic acid ( $10\mu M$ ) for 24 hours ( $n=3$  per group). (I) Human  $iT_{reg}$  cells were treated with or without gallic acid ( $10\mu M$ ) for 48 hours. Cells were treated with MG132 for 6 hours before collection. Cell lysates were immunoprecipitated with anti-Ubiquitin antibody and ubiquitinated FOXP3 levels were detected by Western blot. (J) Flow cytometric analysis of CellTrace Violet-labeled effector T  $T_{eff}$  cells cultured with  $iT_{reg}$  cells that were pre-treated with or without gallic acid ( $10\mu M$ ) at the indicated  $T_{reg}$ -to- $T_{eff}$  ratios in the presence of anti-CD3/CD28 beads for 3 days. (K) Percentages of proliferating  $T_{eff}$  cells ( $n=3$  for each group). (L) Kaplan-Meier overall survival curve of CRC patients based on *Usp21* gene expression (from TCGA). (M) Representative figure shown the expression of FOXP3 and IFN- $\gamma$  by  $CD4^+$  T cells from peripheral blood mononuclear cells (PBMCs) and single cells of paratumor and tumor tissues of CRC patients, which were treated with or without gallic acid ( $10\mu M$ ) for 24 hours ( $n=6$  per group). (N) Percentages of  $CD4^+$ Foxp3 $^+$   $T_{reg}$  cells as indicated in (M). (O) percentages of IFN- $\gamma^+$ FOXP3 $^+$   $T_{reg}$  cells as indicated in (M). Results are representative of two (I) and three (G) independent experiments. Data are mean $\pm$ SD; NS, not significant; \* $p<0.05$ , \*\* $p<0.01$ , \*\*\* $p<0.001$ , \*\*\*\* $p<0.0001$  as determined by unpaired two-tailed Student's t-test. CRC, colorectal cancer; p-STAT3, phosphorylated STAT3; q-PCR, quantitative PCR.

$T_{reg}$  cells, including *Rnf31*, *Mdm2*, *Stub1*, *Cblb*, *Usp7*, *Usp21*, *Usp22* and *Usp44*. We observed that gallic acid specifically suppressed the transcription of *Usp21* gene (figure 1F). Taken together, gallic acid potentially induced Th1-like  $FOXP3^{lo}$   $T_{reg}$  cells by dampening the expression of *Usp21* gene.

As p-STAT3 drives *Usp21* gene transcription.<sup>30</sup> We next tested the effects of gallic acid on STAT3 phosphorylation. Gallic acid inhibited STAT3 phosphorylation at Y705 site (figure 1G) and prevented the binding of p-STAT3 (p-STAT3) to *Usp21* gene promoter (figure 1H). These data suggested that gallic acid suppressed *Usp21* gene transcription by inhibiting STAT3 phosphorylation.

Gallic acid suppressed *Usp21* gene expression and might promote FOXP3 degradation through poly-ubiquitination. Indeed, we observed higher levels of ubiquitinated FOXP3 in  $T_{reg}$  cells after gallic acid treatment (figure 1I). Since FOXP3 critically maintains  $T_{reg}$  cell function.<sup>31</sup> We next examined whether gallic acid perturbed suppressive capacity of  $T_{reg}$  cells. Using an in vitro suppression assay, we found that gallic acid-treated  $T_{reg}$  cells had significantly impaired suppressive capacity towards  $CD4^{+}FOXP3^{-}$  effector T ( $T_{eff}$ ) cell proliferation (figure 1J,K). These results collectively suggested that gallic acid promoted FOXP3 degradation and dampened the suppressive function of  $T_{reg}$  cells.

With respect to CRC, patients with higher levels of *Usp21* transcripts in tumor displayed worse overall survival (OS) (figure 1L). Conceivably, gallic acid suppressed *Usp21* gene expression and potentially promoted better prognosis of CRC patients. To test the potential effects of gallic acid on CRC, peripheral blood mononuclear cells (PBMCs) and single cells of paratumor and tumor tissues from CRC patients were next treated with gallic acid. Interestingly, gallic acid induced FOXP3 loss by  $T_{reg}$  cells (figure 1M–N) and simultaneously induced Th1-like  $T_{reg}$  cells in blood, paratumor and tumor samples, which was characterized by increased percentages of  $IFN-\gamma^{+}FOXP3^{lo}$   $T_{reg}$  cells (figure 1M,O). Overall, these results supported that gallic acid induced Th1-like  $FOXP3^{lo}$   $T_{reg}$  cells by repressing *Usp21* gene transcription.

In summary, we found that gallic acid inhibited *Usp21* expression by decreasing STAT3 phosphorylation. *Usp21* further dampened FOXP3 stability and induced Th1-like  $FOXP3^{lo}$   $T_{reg}$  cells.

### Gallic acid prevents subcutaneous tumor growth

As previously outlined, gallic acid induced instable  $FOXP3^{lo}$   $T_{reg}$  cells and might promote antitumor immunity to restrain tumor growth. Thus, we first tested the antitumor effects of gallic acid in subcutaneous tumor models. Indeed, gallic acid greatly suppressed the growth of syngeneic MC38 colorectal adenocarcinoma cells (figure 2A), B16F10 melanoma cells (figure 2E) and 4T1 mammary carcinoma cells (figure 2I). Overall, gallic acid significantly prevented subcutaneous tumor growth.

To investigate in vivo influences of gallic acid on the stability of  $T_{reg}$  cells and their suppressive capacity towards

PD-1<sup>+</sup> cytotoxic T cells, we next analyzed Foxp3 and PD-L1 expression using flow cytometry. Notably, we observed decreased frequencies of Foxp3<sup>+</sup> and Foxp3<sup>+</sup>PD-L1<sup>+</sup> intra-tumoral  $T_{reg}$  cells on gallic acid treatment (online supplemental figure 4A–F), which was simultaneously accompanied with much lower protein levels of Foxp3 and PD-L1 in  $T_{reg}$  cells from subcutaneous MC38 tumor (figure 2B–D), B16F10 tumor (figure 2F–H) and 4T1 tumor (figure 2J–L). Taken together, gallic acid restricted subcutaneous tumor growth by inhibiting Foxp3 and PD-L1 expression in intra-tumoral  $T_{reg}$  cells, which might further promote antitumor immunity.

### Usp21-deficient $T_{reg}$ cells prevent subcutaneous tumor growth

To study the physiological roles of *Usp21* in intra-tumoral  $T_{reg}$  cells, we next generated a subcutaneous MC38 tumor model in *Usp21<sup>fl/fl</sup>Foxp3<sup>cre</sup>* and *Foxp3<sup>cre</sup>* mice. *Usp21<sup>fl/fl</sup>Foxp3<sup>cre</sup>* mice displayed attenuated tumor growth, which was characterized by smaller MC38 tumor sizes (figure 3A,B). Compared with *Foxp3<sup>cre</sup>* mice, we observed decreased percentages of  $CD4^{+}Foxp3^{+}$   $T_{reg}$  cells in *Usp21<sup>fl/fl</sup>Foxp3<sup>cre</sup>* mice (online supplemental figure 4G). Moreover, *Usp21*-deficient  $T_{reg}$  cells, had much lower levels of Foxp3 protein (figure 3C,D) but higher levels of IFN- $\gamma$  (figure 3F), which significantly promoted IFN- $\gamma$  expression by  $CD4^{+}Foxp3^{-}$   $T_{eff}$  cells (figure 3G). Therefore, *Usp21*-deficient  $T_{reg}$  cells, expressed lower Foxp3, became Th1-like, which amplified Th1 responses and limited subcutaneous tumor growth.

We next tested whether *Usp21* perturbed intra-tumoral  $T_{reg}$  cell's expression of PD-L1 protein. Compared with WT  $T_{reg}$  cells, we observed much lower levels of PD-L1 in *Usp21*-deficient counterparts (figure 3G), which were characterized by lower percentages of PD-L1<sup>+</sup>Foxp3<sup>+</sup>  $T_{reg}$  cells (online supplemental figure 4H) and decreased mean fluorescent intensity (MFI) of PD-L1 (figure 3H). Moreover, tumor infiltrating  $CD8^{+}$  cytotoxic T cells produced higher amounts of IFN- $\gamma$  in *Usp21<sup>fl/fl</sup>Foxp3<sup>cre</sup>* mice (figure 3I,J), while expressed lower levels of PD-1 (figure 3I,K), possibly due to loss of Foxp3 and PD-L1 in *Usp21*-deficient  $T_{reg}$  cells. Taken together, these results revealed that *Usp21*-deficient  $T_{reg}$  cells amplified Th1 phenotype and cytotoxic T cell responses and prevented subcutaneous MC38 tumor growth.

### Usp21-deficient $T_{reg}$ cells prevent colorectal carcinogenesis

To confirm the role of *Usp21*-deficient  $T_{reg}$  cells in CRC progression, we generated an AOM-DSS-induced murine CRC model in *Usp21<sup>fl/fl</sup>Foxp3<sup>cre</sup>* and *Foxp3<sup>cre</sup>* mice. Interestingly, compared with *Foxp3<sup>cre</sup>* mice, *Usp21<sup>fl/fl</sup>Foxp3<sup>cre</sup>* mice developed less colorectal tumors in middle and distal colon regions (figure 4A,B). Statistical analysis further confirmed that colorectal tumor numbers and sizes dramatically decreased in *Usp21<sup>fl/fl</sup>Foxp3<sup>cre</sup>* mice (figure 4C,D). Together, *Usp21*-deficient  $T_{reg}$  cells prevent colorectal carcinogenesis in vivo.

In *Usp21<sup>fl/fl</sup>Foxp3<sup>cre</sup>* mice, we further observed decreased percentages of  $CD4^{+}Foxp3^{+}$   $T_{reg}$  cells (figure 4E, online supplemental figure 4I), with lower levels of Foxp3

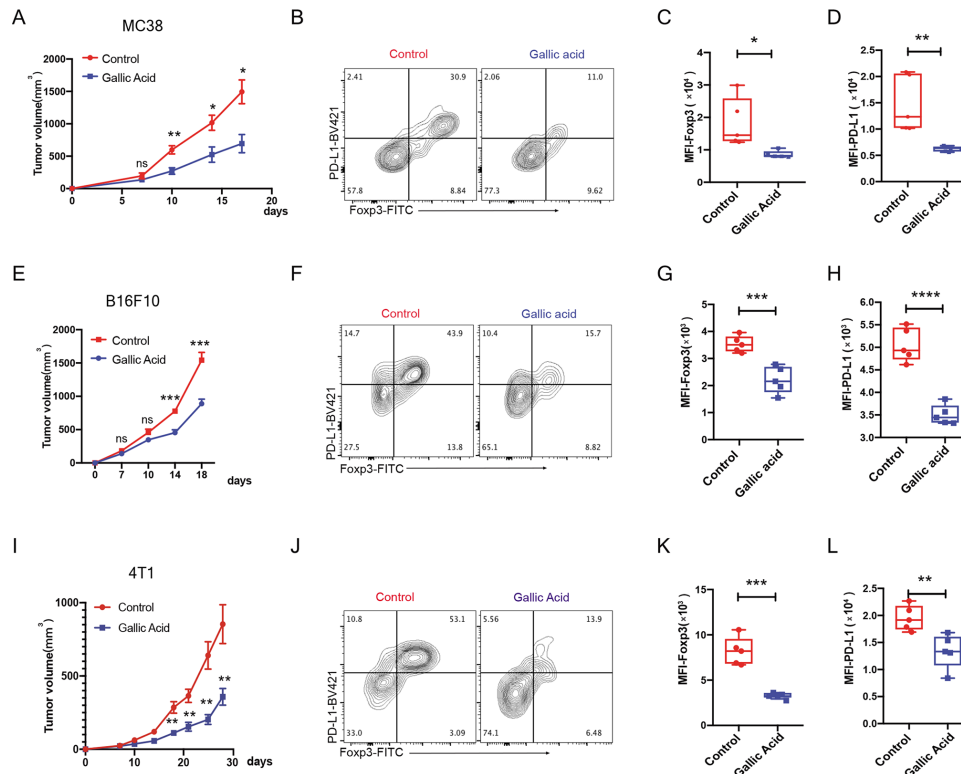


**Figure 2** Gallic acid prevents subcutaneous MC38 tumor growth. (A) MC38 tumor volume of WT mice intraperitoneally treated with or without gallic acid (5 mg/kg) daily, starting at day 7. Tumor volume was measured every 3 or 4 days ( $n=5$  per group). (B) Representative figure shown the expression of Foxp3 and PD-L1 by tumor infiltrating  $CD4^+$  T cells in MC38 tumors, as indicated in (A). (C, D) Mean fluorescent intensity (MFI) of Foxp3 (C) and PD-L1 (D) in  $T_{reg}$  cells as indicated in (B). (E) B16F10 tumor volume of WT mice intraperitoneally treated with or without gallic acid (5 mg/kg) daily, starting at day 7. Tumor volume was measured every 3 or 4 days ( $n=5$  per group). (F) Representative figure shown the expression of Foxp3 and PD-L1 by tumor infiltrating  $CD4^+$  T cells in B16F10 tumors, as indicated in (E). (G, H) MFI of Foxp3 (G) and PD-L1 (H) in  $T_{reg}$  cells as indicated in (F). (I) 4T1 tumor volume of WT mice intraperitoneally treated with or without gallic acid (5 mg/kg) daily, starting at day 7. tumor volume was measured every 3 or 4 days ( $n=5$  per group). (J) Representative figure shown the expression of Foxp3 and PD-L1 by tumor infiltrating  $CD4^+$  T cells in 4T1 tumors, as indicated in (I). (J, K) MFI of Foxp3 (J) and PD-L1 (K) in  $T_{reg}$  cells as indicated in (J). Data are mean $\pm$ SD; NS, not significant; \* $p<0.05$ , \*\* $p<0.01$ , \*\*\* $p<0.001$ , \*\*\*\* $p<0.0001$  as determined by unpaired two-tailed Student's t-test. WT, wild-type.

protein (figure 4F). Meanwhile, Usp21-deficient  $T_{reg}$  cells expressed much lower levels of PD-L1 (figure 4G, (online supplemental figure 4J), suggesting regulatory roles of Usp21 in PD-L1 expression. In parallel with previous results,  $CD4^+Foxp3^+$  Usp21-deficient  $T_{reg}$  cells became Th1-like and produced increased levels of IFN- $\gamma$  (figure 4H,I). Moreover, tumor infiltrating  $CD8^+$  cytotoxic T cells produced higher amounts of IFN- $\gamma$  and expressed much lower levels of PD-1 in *Usp21*<sup>fl/fl</sup>*Foxp3*<sup>cre</sup> mice (figure 4J–L), possibly due to impaired suppressive activity of Usp21-deficient  $T_{reg}$  cells.<sup>21</sup> These findings convinced that Usp21-deficient  $T_{reg}$  cells significantly prevented AOM-DSS-induced colorectal carcinogenesis.

#### Gallic acid downregulates PD-L1 through inhibiting USP21 mediated deubiquitination

Previous data suggested that PD-L1 protein level was decreased in gallic acid-treated and Usp21-deficient  $T_{reg}$  cells, and we observed that *Pdcd1* gene was still actively transcribed (figure 5A), while Usp21 and PD-L1 protein were downregulated in Usp21-deficient  $T_{reg}$  cells

(figure 5B), suggesting PD-L1 protein stability potentially through post-translational modification. Our data revealed ubiquitination-mediated degradation of PD-L1.

We studied the half-life of PD-L1 using the protein synthesis inhibitor cycloheximide. Ectopically expressed Usp21 significantly extended the half-life of PD-L1 protein (figure 5C). To test whether Usp21 functioned as a direct E3 deubiquitinase of PD-L1, we next carried out binding studies to determine whether PD-L1 could bind to Usp21. Reciprocal immunoprecipitation of FLAG-PD-L1 and MYC-Usp21 revealed an interaction between Usp21 and PD-L1 (figure 5D). We also detected the endogenous interaction between Usp21 and PD-L1 in human  $T_{reg}$  cells (figure 5E) and LOVO cancer cells (figure 5F). These data further suggested regulatory roles of Usp21, in  $T_{reg}$  cells, were carried out through interacting with PD-L1.

Using a His-ubiquitin pulldown assay, we found that ectopically expressed Usp21, but not the enzymatically inactive mutant C221A, reduced levels of ubiquitinated PD-L1 (figure 5G). To identify the specific lysine residues

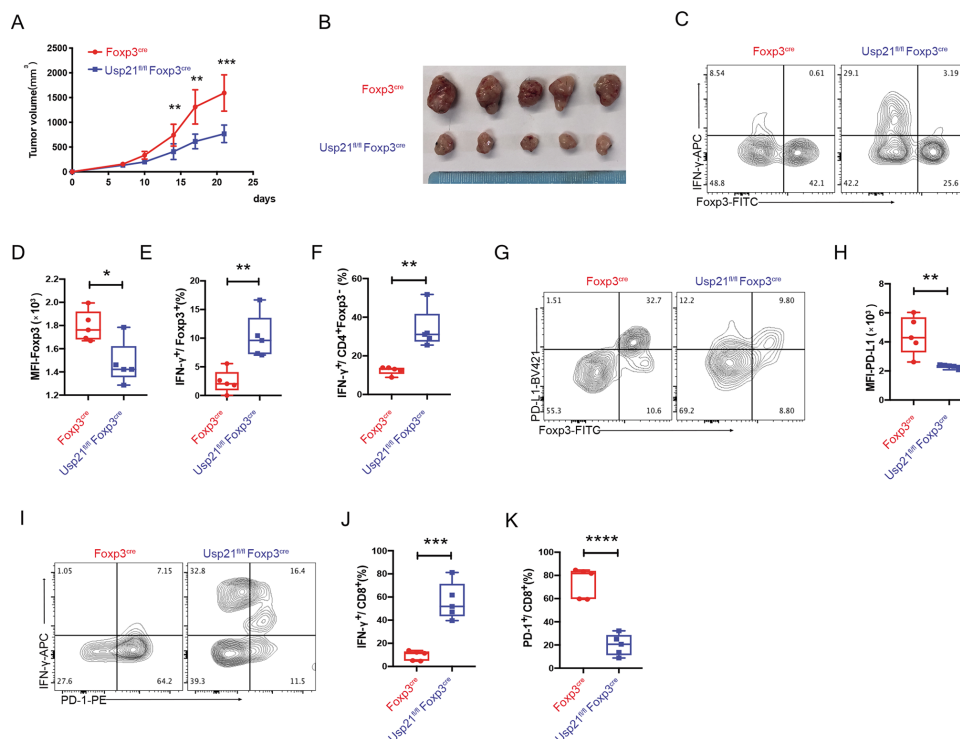


**Figure 3** Usp21-deficient  $T_{reg}$  cells prevent subcutaneous MC38 tumor growth. (A)  $2 \times 10^5$  MC38 colon carcinoma cells were subcutaneously injected into the shaved flanks of  $Foxp3^{Cre}$  or  $Usp21^{fl/fl}Foxp3^{Cre}$  mice ( $n=7$  mice per group). Tumor volume was measured every 3 or 4 days ( $n=5$  per group). (B) Representative tumor image was shown after 21 days, as indicated in (A). (C) representative figure shown the expression of Foxp3 and IFN- $\gamma$  by tumor infiltrating  $CD4^+$  T cells in MC38 tumors, as indicated in (A). (D) Mean fluorescent intensity (MFI) of Foxp3 in  $T_{reg}$  cells as indicated in (C). (E) percentages of IFN- $\gamma^+$ Foxp3 $^+$   $T_{reg}$  cells as indicated in (C). (F) percentages of IFN- $\gamma^+$ Foxp3 $^-$   $T_{reg}$  cells as indicated in (C). (G) representative figure shown the expression of Foxp3 and PD-L1 by tumor infiltrating  $CD4^+$  T cells in MC38 tumors, as indicated in (A). (H) MFI of PD-L1 in  $T_{reg}$  cells as indicated in (G). (I) Representative figure shown the expression of PD-1 and IFN- $\gamma$  by tumor infiltrating  $CD8^+$  T cells in MC38 tumors, as indicated in (A). (J) percentages of  $CD8^+$ IFN- $\gamma^+$  T cells as indicated in (I). (K) percentages of  $CD8^+$ PD-1 $^+$  T cells as indicated in (I). Data are mean $\pm$ SD; NS, not significant; \* $p<0.05$ , \*\* $p<0.01$ , \*\*\* $p<0.001$ , as determined by unpaired two-tailed Student's t-test.

of PD-L1 that could be deubiquitinated by Usp21, we screened each individual lysine-only mutants of PD-L1 (where all lysines within the intracellular regions of PD-L1 were mutated to arginines with only one lysine untouched) and identified three lysine residues (K271, K280 and K281), which were potential Usp21 targets (figure 5H). We further tested mutants where only three lysine residues (K271, K280 and K281) were retained or mutated into arginines (termed K271/280/281 only and K271/280/281R mutants, respectively, figure 5I). His-ubiquitin pull-down assays further confirmed that Usp21 could deubiquitinate PD-L1 at these three lysine residues and the K271/280/281R construct was unresponsive to Usp21-mediated deubiquitination (figure 5I). Furthermore, Usp21 removed K48-linked ubiquitin chain of PD-L1 (figure 5J). These findings demonstrated that Usp21 could stabilize PD-L1 through deubiquitination in  $T_{reg}$  cells.

Next, we observed the downregulation of PD-L1 in gallic acid treated Treg, while *Pdcd1* gene was still actively transcribed (online supplemental figure 3A). Importantly, ectopic Usp21 expression restores Foxp3 and PD-L1 protein expression in Treg cells during gallic acid

treatment (online supplemental figure 3B). Gallic acid treatment significantly shortened the half-life of PD-L1 protein (online supplemental figure 3C), and proteasome inhibition MG132 stabilized PD-L1 during gallic acid treatment (online supplemental figure 3D). Taken together, gallic acid downregulates PD-L1 through inhibiting Usp21 mediated deubiquitination.

### Gallic acid strengthens anti-PD-1 efficacy in subcutaneous tumor model

We further asked whether additional gallic acid treatment improved ICB efficacy in a subcutaneous MC38 tumor model. MC38 tumor-bearing mice were treated with isotype control, gallic acid, anti-PD-1 or gallic acid combined with anti-PD-1 antibody. Gallic acid as well as anti-PD-1 administration prevented MC38 tumor growth and reduced tumor sizes (figure 6A,B), while the combined gallic acid and anti-PD-1 treatment more significantly limited MC38 tumor growth (figure 6A,B) and extended the OS of MC38 tumor-bearing mice (figure 6C). These data suggested that gallic acid strengthened anti-PD-1 efficacy.



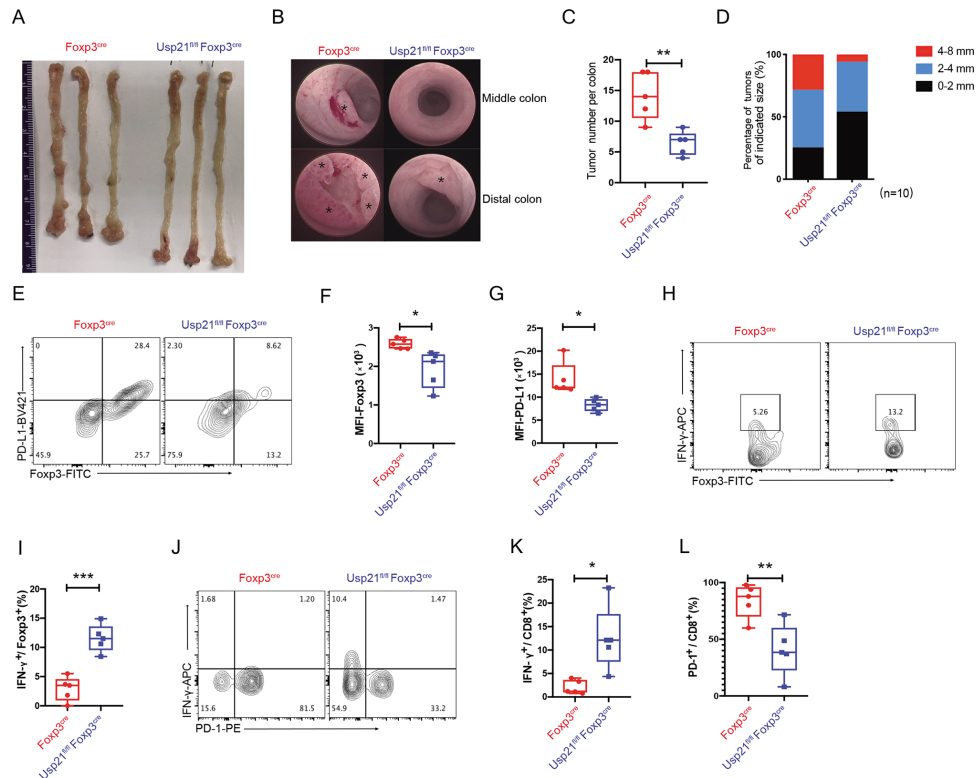


**Figure 4** Usp21-deficient T<sub>reg</sub> cells prevent AOM-DSS-induced colorectal carcinogenesis. (A) Representative figures of dissected colons from *Foxp3<sup>Cre</sup>* and *Usp21<sup>fl/fl</sup>Foxp3<sup>Cre</sup>* mice on day 100 after AOM treatment (n=3 per group). (B) Endoscopic analysis of *Foxp3<sup>Cre</sup>* (n=5) and *Usp21<sup>fl/fl</sup>Foxp3<sup>Cre</sup>* mice (n=5) on day 80 after AOM treatment. (C, D) Tumor number (C) and size distribution (D) of colonic polyps induced by AOM-DSS in *Foxp3<sup>Cre</sup>* (n=5) and *Usp21<sup>fl/fl</sup>Foxp3<sup>Cre</sup>* (n=5) mice. (E) Representative figure shown the expression of Foxp3 and PD-L1 by CD4<sup>+</sup> T cells in colorectal tumors (n=5 per group), as indicated in (A). (F) Mean fluorescent intensity (MFI) of Foxp3 in T<sub>reg</sub> cells as indicated in (E). (G) MFI of PD-L1 in T<sub>reg</sub> cells as indicated in (E). (H) representative figure shown the expression of IFN-γ by CD4<sup>+</sup>Foxp3<sup>+</sup> T<sub>reg</sub> cells in colorectal tumors (n=5 per group), as indicated in (A). (I) Percentages of IFN-γ<sup>+</sup>Foxp3<sup>+</sup> T<sub>reg</sub> cells as indicated in (H). (J) Representative figure shown the expression of PD-1 and IFN-γ by CD8<sup>+</sup> T cells in colorectal tumors (n=5 per group), as indicated in (A). (K) percentages of CD8<sup>+</sup>IFN-γ<sup>+</sup> T cells as indicated in (J). (L) Percentages of CD8<sup>+</sup>PD-1<sup>+</sup> T cells as indicated in (J). Data are mean±SD; NS, not significant; \*p<0.05, \*\*p<0.01, \*\*\*p<0.001, as determined by unpaired two-tailed Student's t-test. AOM, azoxymethane; DSS, dextran sodium sulfate.

In parallel with previous findings, gallic acid significantly induced instable Foxp3 and PD-L1 expression by intratumoral T<sub>reg</sub> cells (figure 6D). In detail, we observed lower percentages of Foxp3<sup>+</sup> or Foxp3<sup>+</sup>PD-L1<sup>+</sup> T<sub>reg</sub> cells (online supplemental figure 4K–L) and decreased MFIs of Foxp3 or PD-L1 among T<sub>reg</sub> cells (figure 6E,F) after gallic acid treatment. Compared with control group, PD-1 blockade slightly decreased Foxp3 and PD-L1 expression by intra-tumoral T<sub>reg</sub> cells, whereas these changes were not statistically significant (figure 6E,F). Moreover, compared with PD-1 blockade group, a combined gallic acid and anti-PD-1 treatment robustly dampened Foxp3 and PD-L1 expression by tumor infiltrating T<sub>reg</sub> cells (figure 6E,F). Together, gallic acid induces the instability of Foxp3 and PD-L1 in intra-tumoral T<sub>reg</sub> cells, while anti-PD-1 antibody does not influence Foxp3 and PD-L1 protein of T<sub>reg</sub> cells.

We next analyzed IFN-γ expression by tumor infiltrating CD4<sup>+</sup>Foxp3<sup>-</sup> T<sub>eff</sub> cells. Compared with control group, gallic acid or PD-1 blockade significantly increased percentages of IFN-γ<sup>+</sup> T<sub>eff</sub> cells in TME (figure 6D,G). Notably, a combined gallic acid and anti-PD-1 treatment enable intra-tumoral T<sub>eff</sub> cells to produce much more

IFN-γ (figure 6D,G), when compared with PD-1 blockade group. Therefore, gallic acid strengthened anti-PD-1 efficacy and restored the function of tumor infiltrating T<sub>eff</sub> cells.

Similar phenotypes were observed in intra-tumoral CD8<sup>+</sup> cytotoxic T cells. Compared with control group, gallic acid or PD-1 blockade significantly increased percentages of CD8<sup>+</sup>IFN-γ<sup>+</sup> cytotoxic T cells in TME (figure 6H,I), while simultaneously dampened PD-1 expression (figure 6H,J). In addition, a combined gallic acid and anti-PD-1 treatment significantly reinvigorated CD8<sup>+</sup> T cells to produce higher amounts of IFN-γ and express lower levels of PD-1 in MC38 tumor (figure 6H–J). Also, we noticed several labs have revealed that TOX is the key regulator of T cell exhaustion. TCR stimulation induces TOX expression, through the NFAT pathway, which further upregulate inhibitory factors PD-1, TIM3, TIGIT and LAG3, associated with decreased IFN-γ and TNF production.<sup>33–34</sup> We have, additionally, measured the protein level of TOX, LAG3 and TNF-α besides IFN-γ and PD-1 to explore the function of gallic acid and anti-PD-1 antibody in T cell

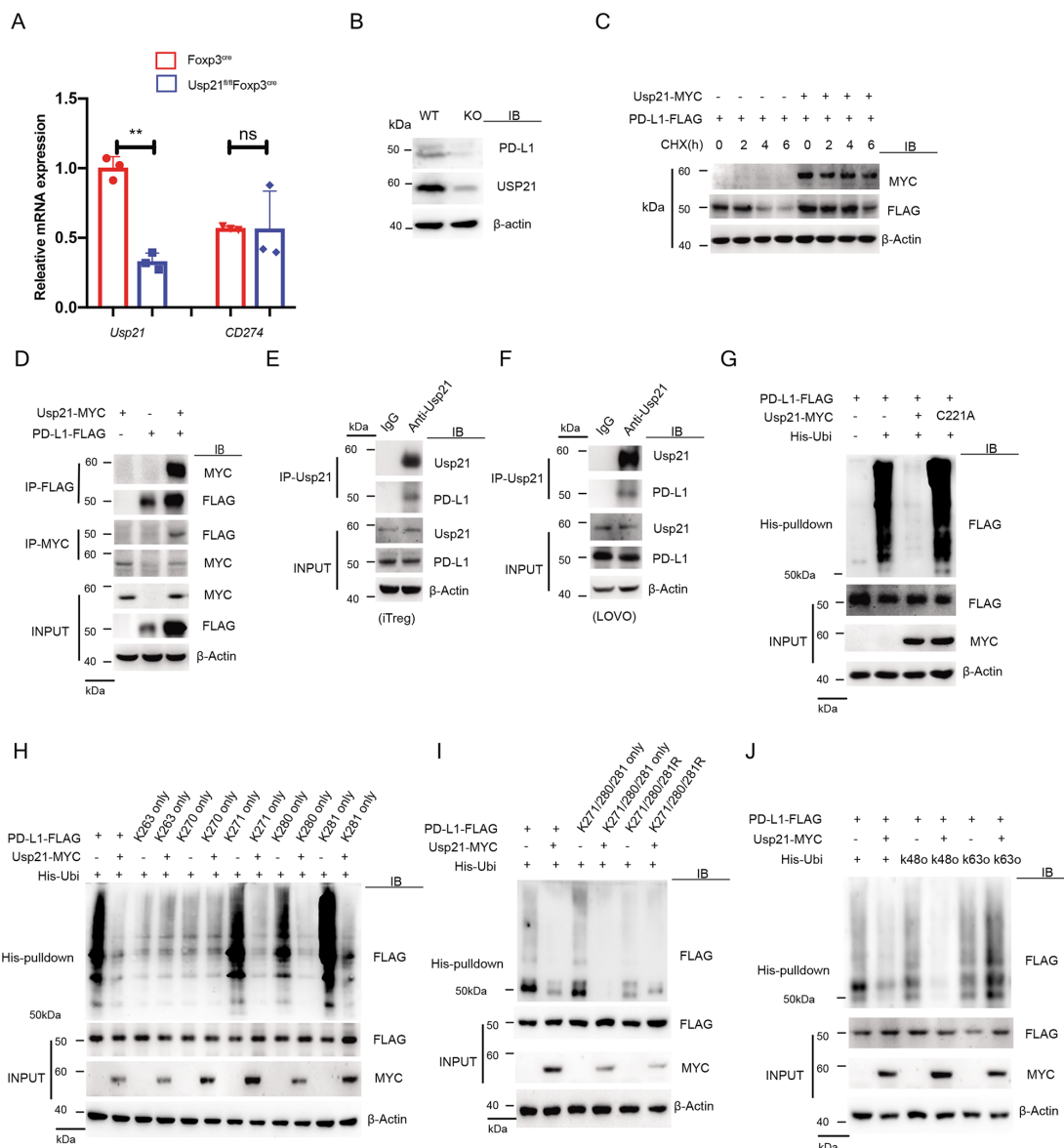


**Figure 5** Usp21 stabilizes PD-L1 through deubiquitination. (A) Relative expression levels of *CD274* mRNA in WT and Usp21-deficient  $T_{reg}$  cells. (B) Representative Western blot shown the expression of PD-L1 protein in WT and Usp21-deficient  $T_{reg}$  cells. (C) HEK293T cells were transfected with control vector, MYC-Usp21 and FLAG-PD-L1 and further treated with cycloheximide (CHX, 10  $\mu$ g/mL) for the indicated time intervals. Protein levels of PD-L1 and USP21 were detected by Western blot. (D) HEK293T cells were cotransfected with FLAG-PD-L1 and MYC-Usp21 and further subjected to immunoprecipitation (IP) with anti-FLAG and anti-MYC antibodies. The immunoprecipitates and lysates were analyzed by Western blot. (E and F) human  $iT_{reg}$  (E) and LoVo cells (F) lysates were immunoprecipitated with anti-Usp21 antibody. The immunoprecipitates and lysates were analyzed by Western blot. (G) HEK293T cells were transfected with indicated constructs and further treated with MG132 for 6 hours before collection. cell lysates were incubated with Ni-NTA beads for 3 hours. Ni-NTA beads were washed and subjected to WB with anti-FLAG. (H) HEK293T cells were transfected with FLAG-PD-L1 mutants (K270only, K271only, K280only, K281only, K263only) and MYC-Usp21. Cell lysates were incubated with Ni-NTA beads for 3 hours. Ni-NTA beads were washed and subjected to WB with anti-FLAG. (I) HEK293T cells were transfected with FLAG-PD-L1 mutants (K271/280/281only, K271/280/281R) and MYC-Usp21. cell lysates were incubated with Ni-NTA beads for 3 hours. Ni-NTA beads were washed and subjected to WB with anti-FLAG. (J) HEK293T cells were transfected with FLAG-PD-L1, MYC-Usp21 and His-Ubi mutants (K48only, K63only). cell lysates were incubated with Ni-NTA beads for 3 hours. Ni-NTA beads were washed and subjected to WB with anti-FLAG. Results are representative of two (B, C, E–J) and three (D) independent experiments. \*\* $p < 0.01$  as determined by unpaired two-tailed Student's t-test. WT, wild-type.

exhaustion. The results showed that TOX and LAG3 expression decreased in  $CD8^+$  T cells,  $TNF-\alpha$  increased in  $CD8^+$  T cells after gallic acid treatment and anti-PD-1 antibody treatment (online supplemental figure

5). Taken together, these results suggested that gallic acid could strengthen ICB efficacy in repressing tumor development.

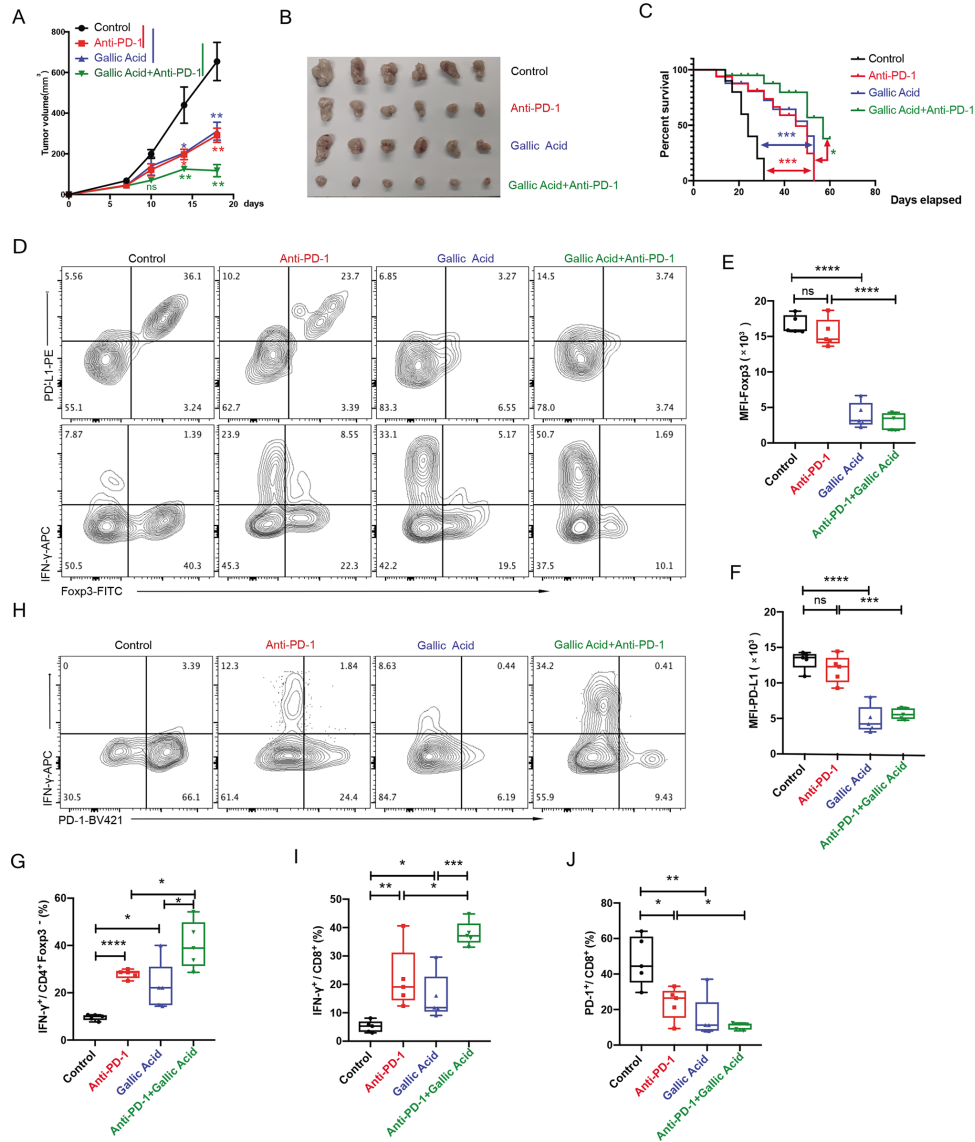


**Figure 6** Gallic acid strengthens anti-PD-1 efficacy in subcutaneous tumor model. (A) MC38 tumor volume of WT mice intraperitoneally treated with isotype control (100  $\mu$ g/injection), anti-PD-1 antibody (100  $\mu$ g/injection), gallic acid (5 mg/kg) or gallic acid (5 mg/kg) plus anti-PD-1 antibody (100  $\mu$ g/injection). tumor volume was measured every three or four days ( $n=6$  per group), as indicated in (A). (C) The survival curve of WT mice in (A). (D) Representative figure shown the expression of Foxp3, PD-L1 and IFN- $\gamma$  by CD4 $^{+}$  T cells in MC38 tumors, as indicated in (A). (E) Mean fluorescent intensity (MFI) of Foxp3 in T<sub>reg</sub> cells ( $n=5$  per group), as indicated in (D). (F) MFI of PD-L1 in T<sub>reg</sub> cells ( $n=5$  per group), as indicated in (D). (G) percentages of IFN- $\gamma^{+}$ Foxp3 $^{-}$  T<sub>eff</sub> cells ( $n=5$  per group), as indicated in (D). (H) representative figure shown the expression of PD-1 and IFN- $\gamma$  by CD8 $^{+}$  T cells in colorectal tumors ( $n=5$  per group), as indicated in (A). (I) Percentages of CD8 $^{+}$ IFN- $\gamma^{+}$  T cells as indicated in (H). (J) Percentages of CD8 $^{+}$ PD-1 $^{+}$  T cells as indicated in (H). Data are mean $\pm$ SD; NS, not significant; \* $p<0.05$ , \*\* $p<0.01$ , \*\*\* $p<0.001$ , as determined by unpaired two-tailed Student's t-test.  $P$  values in (C) were determined by log-rank test. WT, wild-type.

In summary, anti-PD-1 antibody repressed the growth of MC38 subcutaneous tumor growth by restoring the function of exhausted tumor infiltrating CD8 $^{+}$  T cells. Gallic acid could strengthen ICB efficacy by dampening the expression of PD-L1 and Foxp3 proteins in T<sub>reg</sub>.

### Gallic acid strengthens anti-PD-1 efficacy in murine CRC model

We next investigated whether gallic acid might improve ICB efficacy in AOM-DSS-induced CRC. To minimize

the potential effects of microbiota differences during ICB therapy, we co-housed mice when inducing CRC following AOM-DSS protocol. CRC-bearing mice were treated with isotype control, gallic acid, anti-PD-1 or gallic acid combined with anti-PD-1 antibody, respectively. Gallic acid or anti-PD-1 administration prevented AOM-DSS-induced colorectal carcinogenesis, while a combined gallic acid and anti-PD-1 treatment more significantly limited CRC progression (figure 7A-C).

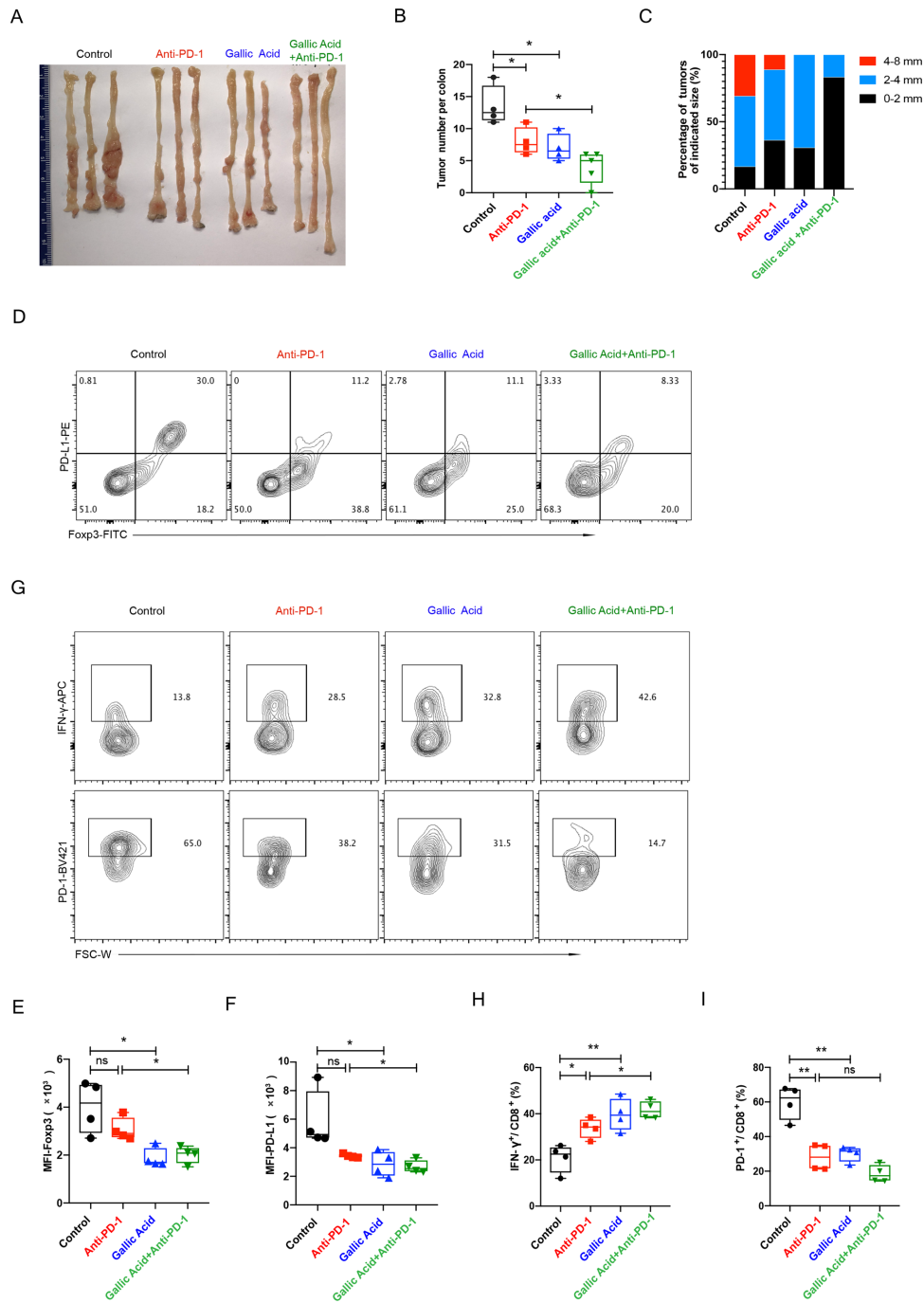


**Figure 7** Gallic acid strengthens anti-PD-1 efficacy in murine CRC model. (A) Representative figures of dissected colons from mice treated with the indicated treatments (n=3 per group). (B, C) Tumor number (B) and size distribution (C) of colonic polyps in mice (isotype control: n=4; anti-PD-1: n=4; gallic acid: n=4; gallic acid plus anti-PD-1: n=5), as indicated in (A). (D) Representative figure shown the expression of Foxp3 and PD-L1 by CD4<sup>+</sup> T cells in colorectal tumors (n=4 per group), as indicated in (A). (E) Mean fluorescent intensity (MFI) of Foxp3 in T<sub>reg</sub> cells as indicated in (D). (F) MFI of PD-L1 in T<sub>reg</sub> cells as indicated in (D). (G) Representative figure shown the expression of IFN-γ and PD-1 by CD8<sup>+</sup> T cells in colorectal tumors (n=4 per group), as indicated in (A). (H) percentages of CD8<sup>+</sup>IFN-γ<sup>+</sup> T cells as indicated in (G). (I) percentages of CD8<sup>+</sup>PD-1<sup>+</sup> T cells as indicated in (G). Data are mean±SD; NS, not significant; \*p<0.05, \*\*p<0.01, \*\*\*p<0.001, as determined by unpaired two-tailed Student's t-test. CRC, colorectal cancer.

Consistently, gallic acid administration significantly induced instability of Foxp3 and PD-L1 in tumor infiltrating T<sub>reg</sub> cells (figure 7D), which were characterized by decreased percentages of Foxp3<sup>+</sup> or Foxp3<sup>+</sup>PD-L1<sup>+</sup> T<sub>reg</sub> cells (online supplemental figure 4M–N) and lower

MFI of Foxp3 or PD-L1 among T<sub>reg</sub> cells (figure 7E,F). Compared with control group, PD-1 blockade slightly decreased percentages of Foxp3<sup>+</sup> or Foxp3<sup>+</sup>PD-L1<sup>+</sup> intra-tumoral T<sub>reg</sub> cells (online supplemental figure 4M–N), without affecting MFI of Foxp3 or PD-L1 (figure 7E,F).

Moreover, compared with PD-1 blockade group, a combined gallic acid and anti-PD-1 treatment robustly dampened Foxp3 and PD-L1 expression by tumor infiltrating  $T_{reg}$  cells in CRC (figure 7E,F). Overall, gallic acid strengthened anti-PD-1 efficacy in AOM-DSS-induced CRC by inducing Foxp3<sup>lo</sup>PD-L1<sup>lo</sup>  $T_{reg}$  cells, which might further reinvigorate tumor infiltrating T cell function.

Compared with control group, gallic acid or PD-1 blockade significantly increased percentages of CD8<sup>+</sup>IFN- $\gamma$ <sup>+</sup> cytotoxic T cells in TME (figure 7G,H), while simultaneously dampened PD-1 expression (figure 7G,I). More importantly, a combined gallic acid and anti-PD-1 treatment significantly promoted CD8<sup>+</sup> T cells to produce higher amounts of IFN- $\gamma$  in CRC (figure 7H). Consistently, TOX and LAG3 expression decreased in CD8<sup>+</sup> T cells, while TNF- $\alpha$  increased in CD8<sup>+</sup> T cells after gallic acid and anti-PD-1 antibody treatments (online supplemental figure 6). Together, these results demonstrated that gallic acid could strengthen ICB efficacy in AOM-DSS-induced CRC model.

In conclusion, we first screened compounds and identified gallic acid specifically induced Th1-like Foxp3<sup>lo</sup>PD-L1<sup>lo</sup>  $T_{reg}$  cells by suppressing *Usp21* gene transcription (online supplemental figure 1). Mechanistically, *Usp21* stabilized Foxp3 and PD-L1 through deubiquitination. Of note, *Usp21*-deficient  $T_{reg}$  cells impaired PD-L1/PD-1 signaling and Foxp3 stability, promoted IFN- $\gamma$  expression by CD8<sup>+</sup> T cells, and limited tumor growth. Next, gallic acid greatly strengthened anti-PD-1 efficacy in both subcutaneous tumor and AOM-DSS-induced CRC models by inducing Th1-like Foxp3<sup>lo</sup>  $T_{reg}$  cells.

## DISCUSSION

Our study suggests that intestinal  $T_{reg}$  cells are potential therapeutic target for immunotherapies to boost anti-tumor immunity and strengthen anti-PD-1 efficacy in CRC treatment. Using murine subcutaneous tumor and AOM-DSS-induced CRC models, we clearly demonstrate that gallic acid induces Th1-like Foxp3<sup>lo</sup>PD-L1<sup>lo</sup>  $T_{reg}$  cells, which are less immune suppressive, reinvigorate anti-tumor T cell responses and ultimately prevent tumor growth. By contrast, Th17-like  $T_{reg}$  cells facilitate Th17 responses, which induce exhausted tumor infiltrating CD8<sup>+</sup> T cells and promote colorectal carcinogenesis.<sup>26</sup> Therefore, dysfunctional T-helper-like  $T_{reg}$  cells are heterogeneous and play disparate roles in controlling tumor progression. Here we found that type two cytokines such as IL-4 and type 17 cytokines such as IL-17 have no significant difference after gallic acid and anti-PD-1 antibody treatment. These data suggested that gallic acid induces Th1-like Treg cells specially.

Gallic acid is a gut microbial metabolite<sup>29</sup> and potentially protects against DSS-induced intestinal injuries.<sup>35</sup> Janus kinases (JAKs) phosphorylate STAT3 at Y705 site and thus promote the dimerization and nuclear translocation of STAT3.<sup>36</sup> Nuclear STAT3 dimers further activate the transcription of target gene.<sup>36</sup> Here, we demonstrate

that gallic acid inhibits STAT3 phosphorylation at Y705 site and prevents the binding of p-STAT3 to *Usp21* gene promoter. However, it remains largely unclear whether and how gallic acid inhibits the kinase activity of JAKs. To really understand whether this is the case, additional kinase activity assays for gallic acid may be required.

Although previous studies have also revealed that gallic acid exhibits anti-carcinogenic effects,<sup>37,38</sup> the mechanism underlying whether and how gallic acid enhances PD-1 blockade therapy remains largely unclear. Here, we reveal gallic acid treatment significantly dampens  $T_{reg}$  cell function by impairing PD-L1/PD-1 signaling and Foxp3 stability, promotes IFN- $\gamma$  expression by CD8<sup>+</sup> T cells, and thus, prevents colorectal carcinogenesis. Notably, gallic acid enhances the ICB efficacy, in CRC, by targeting *Usp21*. These studies contribute to a better understanding of the roles of *Usp21* in tumor infiltrating  $T_{reg}$  cells from CRC. Overall, our studies provide a unique molecular mechanism and rationale for combining *Usp21* inhibition with PD-1 blockade as an effective immunotherapy for cancer.

Ample studies have demonstrated the regulatory roles of *Usp21* in tumor incidence and progression. For instance, *Usp21* critically promotes hepatocellular carcinoma development by stabilizing MEK2<sup>39</sup> and drives CRC metastasis by regulating Fra-1.<sup>40</sup> Meanwhile, *Usp21* activates Wnt- $\beta$ -catenin pathway and maintains cancer cell stemness.<sup>41</sup> Here, we newly reveal that *Usp21* stabilizes and deubiquitinates PD-L1 at K271, K280 and K280 sites. Meanwhile, *Usp21* interacts with PD-L1 in human LOVO cancer cells. These results suggest that gallic acid directly dampens PD-L1 expression by tumor cells and further prevents PD-L1-mediated immune tolerance. In addition, IFN- $\gamma$  has significant antitumor properties, however, it also simultaneously activates PD-L1 expression to promote tumor resistance to PD-1 blockade immunotherapy.<sup>42,43</sup> Conceivably, gallic acid may simultaneously overcome the pro-tumorigenic effects of IFN- $\gamma$  by promoting PD-L1 degradation, leading to improved ICB efficacy in cancer immunotherapy.

The TME harbors cancer cells and other cells that contribute to tumor development and progression. Consequently, targeting and manipulating the cells in the TME during cancer treatment can help control malignancies and achieve positive health outcomes. We had demonstrated that gallic acid represses CRC development by targeting Treg cells. However, It remains unclear whether gallic acid mediated effects through Treg cell independent mechanisms. Our unpublished data revealed that gallic acid treatment downregulates PD-L1 protein level in human CRC (LOVO) cells, however, gallic acid does not influence the proliferation and migration of tumor cells. Further works should be focus on the additional roles for gallic acid in non-Treg cells.

Our study originality revealed that gallic acid inhibits *Usp21* expression by decreasing STAT3 phosphorylation, further dampens FOXP3 stability and induces Th1-like Foxp3<sup>lo</sup>  $T_{reg}$  cells. Our results elucidate the mechanisms for gallic acid to repress CRC development and

strengthen anti-PD-1 blockade efficacy. However, the underlining mechanisms for gallic acid to inhibit STAT3 phosphorylation need to be further explored. Moreover, we will focus on clarifying the functions of gallic acid and the homeostasis of intestinal flora it associated with .

#### Author affiliations

<sup>1</sup>Center for Immune-Related Diseases at Shanghai Institute of Immunology, Department of Respiratory and Critical Care Medicine of Ruijin Hospital, Department of Immunology and Microbiology, Shanghai Jiao Tong University School of Medicine, Shanghai, China

<sup>2</sup>Department of Medical Oncology, Shanghai Changzheng Hospital, Naval Medical University, Shanghai, China

<sup>3</sup>Shanghai Affinity Biopharmaceutical Co., Ltd, Shanghai, China

<sup>4</sup>Shanghai Jiao Tong University School of Medicine Affiliated Renji Hospital, Shanghai, China

<sup>5</sup>Department of Thoracic Surgery, RuiJin Hospital, Shanghai Jiao Tong University School of Medicine, Shanghai, China

<sup>6</sup>Fudan University School of Basic Medical Sciences, Shanghai, China

<sup>7</sup>Unit of Immune and Metabolic Regulation, School of Life Science and Technology, ShanghaiTech University, Shanghai, China

<sup>8</sup>Department of Thoracic Surgery, Clinical Translational Research Center, Shanghai Pulmonary Hospital, Shanghai, China

<sup>9</sup>Department of Integrated TCM and Western Medicine, Shanghai Skin Disease Hospital, Tongji University School of Medicine, Shanghai, China

<sup>10</sup>Institute of Arthritis Research, Guanghua Integrative Medicine Hospital, Shanghai University of Traditional Chinese Medicine, Shanghai, China

<sup>11</sup>Shenzhen Key Laboratory of Immunity and Inflammatory Diseases, Shenzhen, Guangdong, China

**Correction notice** This article has been corrected since it was first published online. The corresponding authors have been updated.

**Acknowledgements** We thank X. Feng for cell sorting and members from Li's laboratory for helpful discussion. We thank for the support from Core Facility of Basic Medical Sciences, Shanghai Jiao Tong University School of Medicine. We thank for the support from the sequencing core at Shanghai Institute of Immunology.

**Contributors** BD and YL designed the study. BD and BY performed the experiments, and analyzed the data. WZ and YG performed the experiments. YZ provided reagent and expertise. YG provided clinical samples. BL and YL supervised the study and are the guarantor of this paper. BD and YL wrote the manuscript with the input from other authors. JC, YY and XD helped the revision stage.

**Funding** Our research is supported by NSFC 31525008, 81830051 and 31961133011; National Key R&D Program of China 2019YFA09006100; Innovative research team of high-level local universities in Shanghai SSMU-ZDCX20180101. BL is a recipient of Shanghai 'Rising Star' program 10QA1407900, CAS '100-talent' program and National Science Foundation for Distinguished Young Scholars 31525008, Program of Shanghai Academic Research Leader 16XD1403800; Shanghai Jiao Tong University (SJTU)-The Chinese University of Hong Kong (CUHK) Joint Research Collaboration Fund and the Fundamental Research Funds for Central Universities. YL is a recipient of National Postdoctoral Program for Innovative Talents BX201700159, China Postdoctoral Science Foundation 2017M621497 and NSFC 31700775.

**Competing interests** YL are cofounder of Biotheus and Chairman of its scientific advisory board. The remaining authors declare no competing interests.

**Patient consent for publication** Consent obtained directly from patient(s)

**Ethics approval** Study protocols were approved by the ethical review committee of Renji Hospital, Shanghai Jiao Tong University School of Medicine (no. 2017-114-CR-02). Participants gave informed consent to participate in the study before taking part.

**Provenance and peer review** Not commissioned; externally peer reviewed.

**Data availability statement** No data are available.

**Supplemental material** This content has been supplied by the author(s). It has not been vetted by BMJ Publishing Group Limited (BMJ) and may not have been peer-reviewed. Any opinions or recommendations discussed are solely those of the author(s) and are not endorsed by BMJ. BMJ disclaims all liability and

responsibility arising from any reliance placed on the content. Where the content includes any translated material, BMJ does not warrant the accuracy and reliability of the translations (including but not limited to local regulations, clinical guidelines, terminology, drug names and drug dosages), and is not responsible for any error and/or omissions arising from translation and adaptation or otherwise.

**Open access** This is an open access article distributed in accordance with the Creative Commons Attribution Non Commercial (CC BY-NC 4.0) license, which permits others to distribute, remix, adapt, build upon this work non-commercially, and license their derivative works on different terms, provided the original work is properly cited, appropriate credit is given, any changes made indicated, and the use is non-commercial. See <http://creativecommons.org/licenses/by-nc/4.0/>.

#### ORCID iDs

Yixian Guo <http://orcid.org/0000-0002-4542-4929>

Yangyang Li <http://orcid.org/0000-0002-5791-9443>

#### REFERENCES

- Salmaninejad A, Valilou SF, Shabgah AG, *et al*. Pd-1/Pd-L1 pathway: basic biology and role in cancer immunotherapy. *J Cell Physiol* 2019;234:16824-37.
- Melief CJ, Kast WM. Efficacy of cytotoxic T lymphocytes against virus-induced tumors. *Cancer Cells* 1990;2:116-20.
- Scott AC, Dündar F, Zumbo P, *et al*. Tox is a critical regulator of tumour-specific T cell differentiation. *Nature* 2019;571:270-4.
- Chen DS, Mellman I. Elements of cancer immunity and the cancer-immune set point. *Nature* 2017;541:321-30.
- Le DT, Durham JN, Smith KN, *et al*. Mismatch repair deficiency predicts response of solid tumors to PD-1 blockade. *Science* 2017;357:409-13.
- Le DT, Uram JN, Wang H, *et al*. Pd-1 blockade in tumors with mismatch-repair deficiency. *N Engl J Med* 2015;372:2509-20.
- Sinicrope FA, Rego RL, Ansell SM, *et al*. Intraepithelial effector (CD3+)/regulatory (FoxP3+) T-cell ratio predicts a clinical outcome of human colon carcinoma. *Gastroenterology* 2009;137:1270-9.
- Saito T, Nishikawa H, Wada H, *et al*. Two FOXP3(+)/CD4(+) T cell subpopulations distinctly control the prognosis of colorectal cancers. *Nat Med* 2016;22:679-84.
- Munn DH, Bronte V. Immune suppressive mechanisms in the tumor microenvironment. *Curr Opin Immunol* 2016;39:1-6.
- Gajewski TF, Schreiber H, Fu Y-X. Innate and adaptive immune cells in the tumor microenvironment. *Nat Immunol* 2013;14:1014-22.
- Binnewies M, Roberts EW, Kersten K, *et al*. Understanding the tumor immune microenvironment (time) for effective therapy. *Nat Med* 2018;24:541-50.
- Kamada T, Togashi Y, Tay C, *et al*. PD-1<sup>+</sup> regulatory T cells amplified by PD-1 blockade promote hyperprogression of cancer. *Proc Natl Acad Sci U S A* 2019;116:9999-10008.
- Sakaguchi S, Mikami N, Wing JB, *et al*. Regulatory T cells and human disease. *Annu Rev Immunol* 2020;38:541-66.
- Sakaguchi S, Yamaguchi T, Nomura T, *et al*. Regulatory T cells and immune tolerance. *Cell* 2008;133:775-87.
- De Simone M, Arrigoni A, Rossetti G, *et al*. Transcriptional landscape of human tissue lymphocytes unveils uniqueness of tumor-infiltrating T regulatory cells. *Immunity* 2016;45:1135-47.
- Sun C, Mezzadra R, Schumacher TN. Regulation and function of the PD-L1 checkpoint. *Immunity* 2018;48:434-52.
- Delgoffe GM, Woo S-R, Turnis ME, *et al*. Stability and function of regulatory T cells is maintained by a neuropilin-1-semaphorin-4a axis. *Nature* 2013;501:252-6.
- Overacre-Delgoffe AE, Chikina M, Dadey RE, *et al*. Interferon- $\gamma$  Drives T<sub>reg</sub> Fragility to Promote Anti-tumor Immunity. *Cell* 2017;169:1130-41.
- Zhou X, Bailey-Bucktrout SL, Jeker LT, *et al*. Instability of the transcription factor FOXP3 leads to the generation of pathogenic memory T cells in vivo. *Nat Immunol* 2009;10:1000-7.
- Chen Z, Barbi J, Bu S, *et al*. The ubiquitin ligase STUB1 negatively modulates regulatory T cell suppressive activity by promoting degradation of the transcription factor FOXP3. *Immunity* 2013;39:272-85.
- Li Y, Lu Y, Wang S, *et al*. USP21 prevents the generation of T-helper-1-like Treg cells. *Nat Commun* 2016;7:13559.
- Yang J, Wei P, Barbi J, *et al*. The deubiquitinase USP44 promotes Treg function during inflammation by preventing FOXP3 degradation. *EMBO Rep* 2020;21:e50308.
- Cortez JT, Montauti E, Shifrut E, *et al*. CRISPR screen in regulatory T cells reveals modulators of Foxp3. *Nature* 2020;582:416-20.
- Wang L, Kumar S, Dahiya S, *et al*. Ubiquitin-specific Protease-7 inhibition impairs Tip60-dependent Foxp3+ T-regulatory cell function and promotes antitumor immunity. *EBioMedicine* 2016;13:99-112.

- 25 Li Y, Li B. A translational perspective of a deubiquitinase inhibitor in antitumor immunity. *EBioMedicine* 2016;13:7–8.
- 26 Lu Y, Li Y, Liu Q, *et al.* MondoA-Thioredoxin-Interacting protein axis maintains regulatory T-cell identity and function in colorectal cancer microenvironment. *Gastroenterology* 2021;161:575–91.
- 27 Gao J, Aksoy BA, Dogrusoz U, *et al.* Integrative analysis of complex cancer genomics and clinical profiles using the cBioPortal. *Sci Signal* 2013;6:pl1.
- 28 Cerami E, Gao J, Dogrusoz U, *et al.* The cBio cancer genomics portal: an open platform for exploring multidimensional cancer genomics data. *Cancer Discov* 2012;2:401–4.
- 29 Kadosh E, Snir-Alkalay I, Venkatachalam A, *et al.* The gut microbiome switches mutant p53 from tumour-suppressive to oncogenic. *Nature* 2020;586:133–8.
- 30 Jin J, Liu J, Chen C, *et al.* The deubiquitinase USP21 maintains the stemness of mouse embryonic stem cells via stabilization of Nanog. *Nat Commun* 2016;7:13594.
- 31 Lu L, Barbi J, Pan F. The regulation of immune tolerance by FOXP3. *Nat Rev Immunol* 2017;17:703–17.
- 32 Seo H, Chen J, González-Avalos E, *et al.* TOX and TOX2 transcription factors cooperate with NR4A transcription factors to impose CD8<sup>+</sup> T cell exhaustion. *Proc Natl Acad Sci U S A* 2019;116:12410–5.
- 33 Kim CG, Jang M, Kim Y, *et al.* Vegf-A drives TOX-dependent T cell exhaustion in anti-PD-1-resistant microsatellite stable colorectal cancers. *Sci Immunol* 2019;4. doi:10.1126/sciimmunol.aay0555. [Epub ahead of print: 08 11 2019].
- 34 Khan O, Giles JR, McDonald S, *et al.* TOX transcriptionally and epigenetically programs CD8<sup>+</sup> T cell exhaustion. *Nature* 2019;571:211–8.
- 35 Pandurangan AK, Mohebbi N, Esa NM, *et al.* Gallic acid suppresses inflammation in dextran sodium sulfate-induced colitis in mice: possible mechanisms. *Int Immunopharmacol* 2015;28:1034–43.
- 36 Levy DE, Lee C-kuo. What does STAT3 do? *J Clin Invest* 2002;109:1143–8.
- 37 Kim SW, Han YW, Lee ST, *et al.* A superoxide anion generator, pyrogallol, inhibits the growth of HeLa cells via cell cycle arrest and apoptosis. *Mol Carcinog* 2008;47:114–25.
- 38 Dong Z, Feng L, Chao Y, *et al.* Amplification of tumor oxidative stresses with liposomal Fenton catalyst and glutathione inhibitor for enhanced cancer chemotherapy and radiotherapy. *Nano Lett* 2019;19:805–15.
- 39 Li W, Cui K, Prochownik EV, *et al.* The deubiquitinase USP21 stabilizes MEK2 to promote tumor growth. *Cell Death Dis* 2018;9:482.
- 40 Yun S-I, Hong HK, Yeo S-Y, *et al.* Ubiquitin-Specific protease 21 promotes colorectal cancer metastasis by acting as a Fra-1 deubiquitinase. *Cancers* 2020;12:207.
- 41 Hou P, Ma X, Zhang Q, *et al.* USP21 deubiquitinase promotes pancreas cancer cell stemness via Wnt pathway activation. *Genes Dev* 2019;33:1361–6.
- 42 Alspach E, Lussier DM, Schreiber RD. Interferon  $\gamma$  and its important roles in promoting and inhibiting spontaneous and therapeutic cancer immunity. *Cold Spring Harb Perspect Biol* 2019;11:a028480.
- 43 Ayers M, Luceford J, Nebozhyn M, *et al.* IFN- $\gamma$ -related mRNA profile predicts clinical response to PD-1 blockade. *J Clin Invest* 2017;127:2930–40.

## Correction: Gallic acid induces T-helper-1-like Treg cells and strengthens immune checkpoint blockade efficacy

Deng B, Yang B, Chen J, *et al.* Gallic acid induces T-helper-1-like Treg cells and strengthens immune checkpoint blockade efficacy. *J Immunother Cancer* 2022;**10**:e004037. doi: 10.1136/jitc-2021-004037

Yuansheng Zang, Yangyang Li and Bin Li have now been listed as co-corresponding authors.

**Open access** This is an open access article distributed in accordance with the Creative Commons Attribution Non Commercial (CC BY-NC 4.0) license, which permits others to distribute, remix, adapt, build upon this work non-commercially, and license their derivative works on different terms, provided the original work is properly cited, appropriate credit is given, any changes made indicated, and the use is non-commercial. See <http://creativecommons.org/licenses/by-nc/4.0/>.

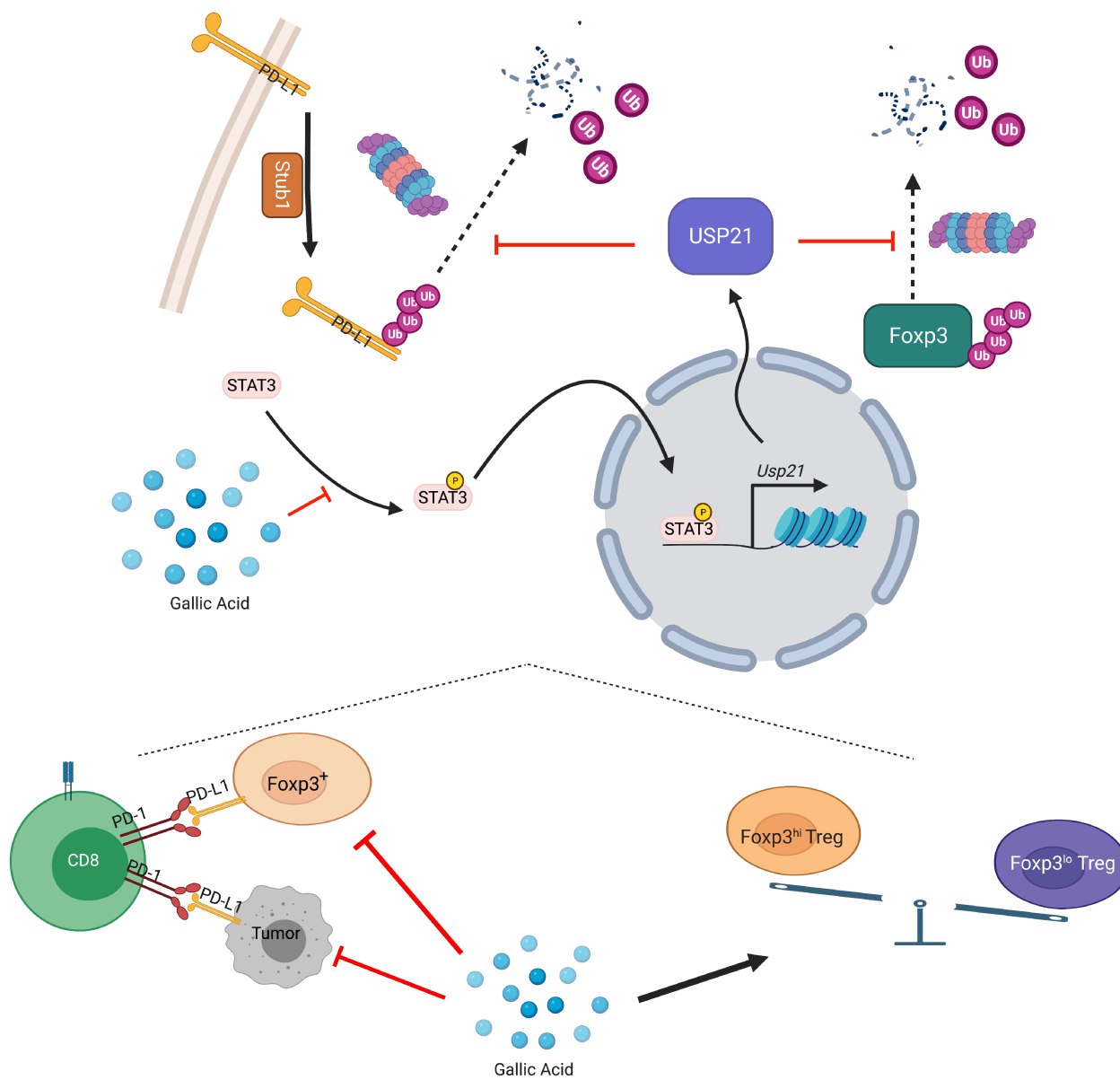
© Author(s) (or their employer(s)) 2022. Re-use permitted under CC BY-NC. No commercial re-use. See rights and permissions. Published by BMJ.

*J Immunother Cancer* 2022;**10**:e004037corr1. doi:10.1136/jitc-2021-004037corr1

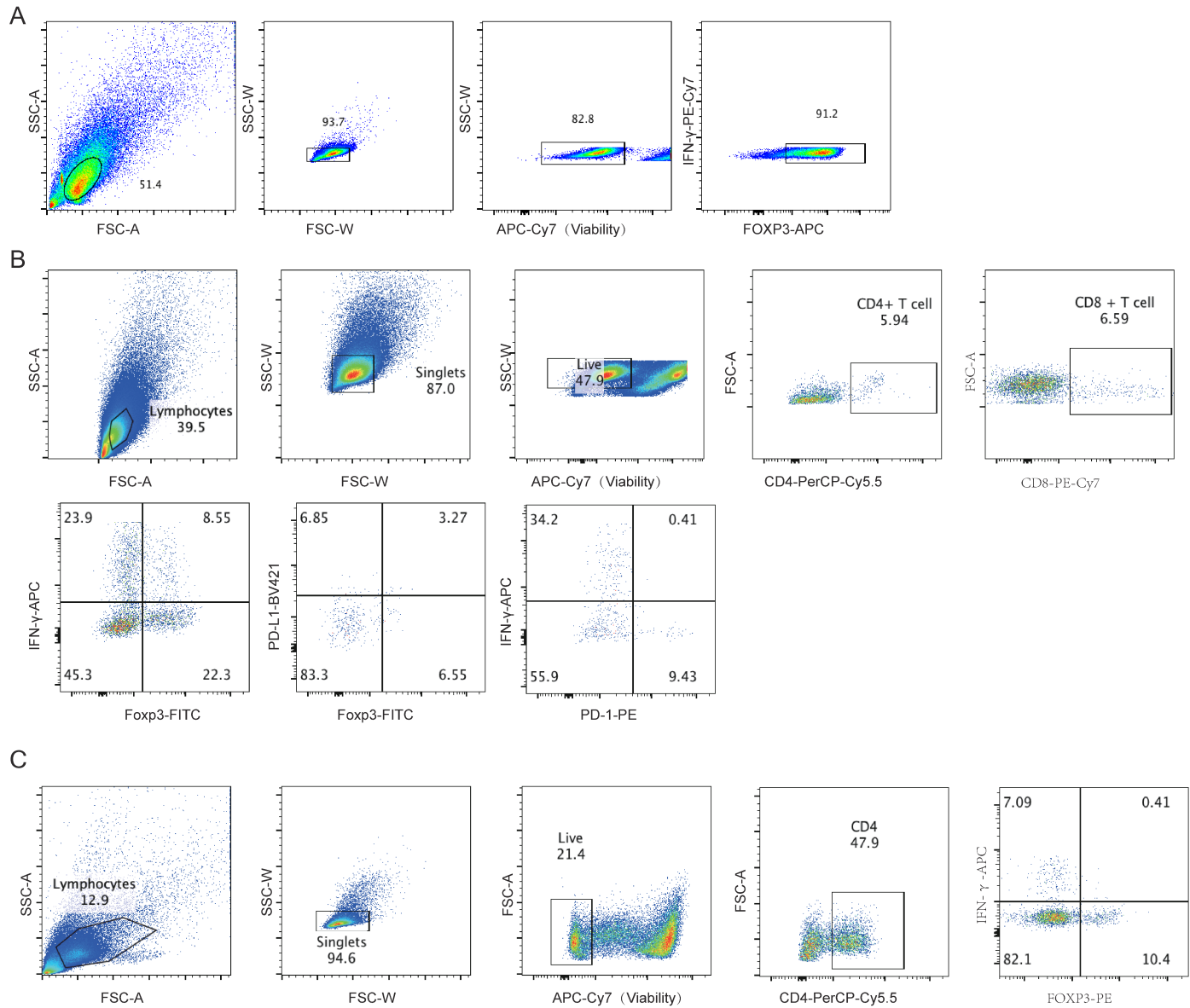


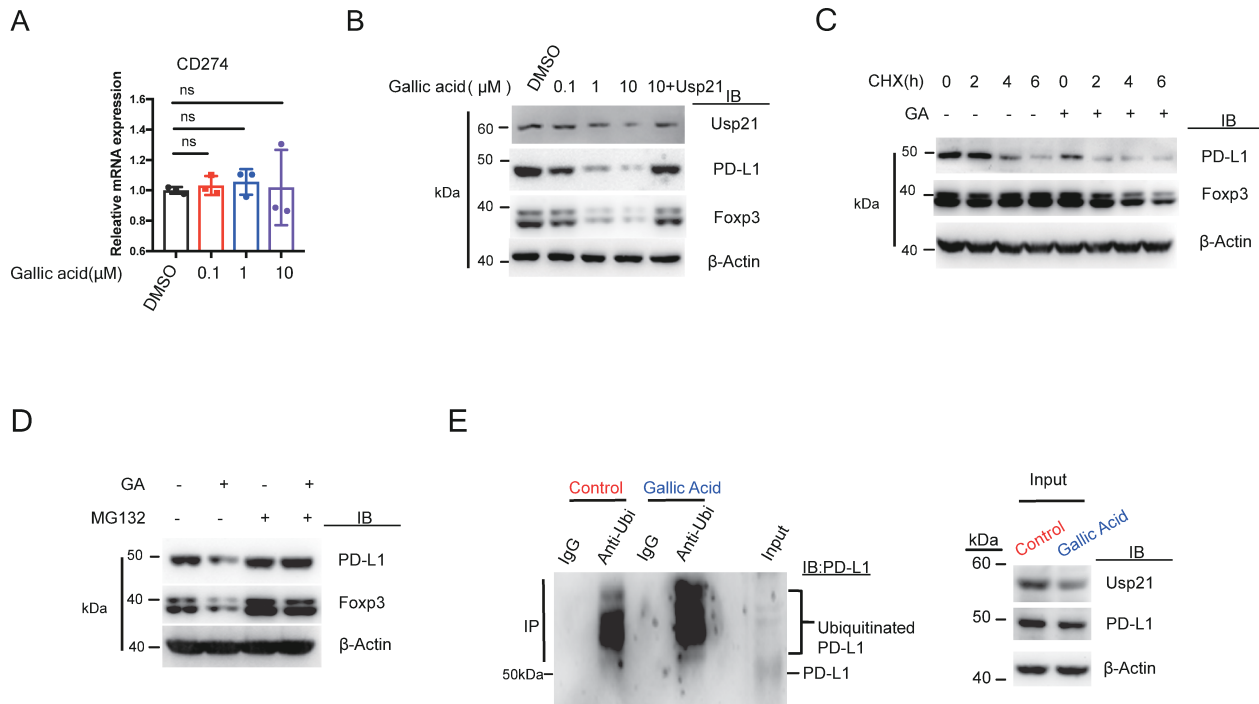


## Supplementary figure 1

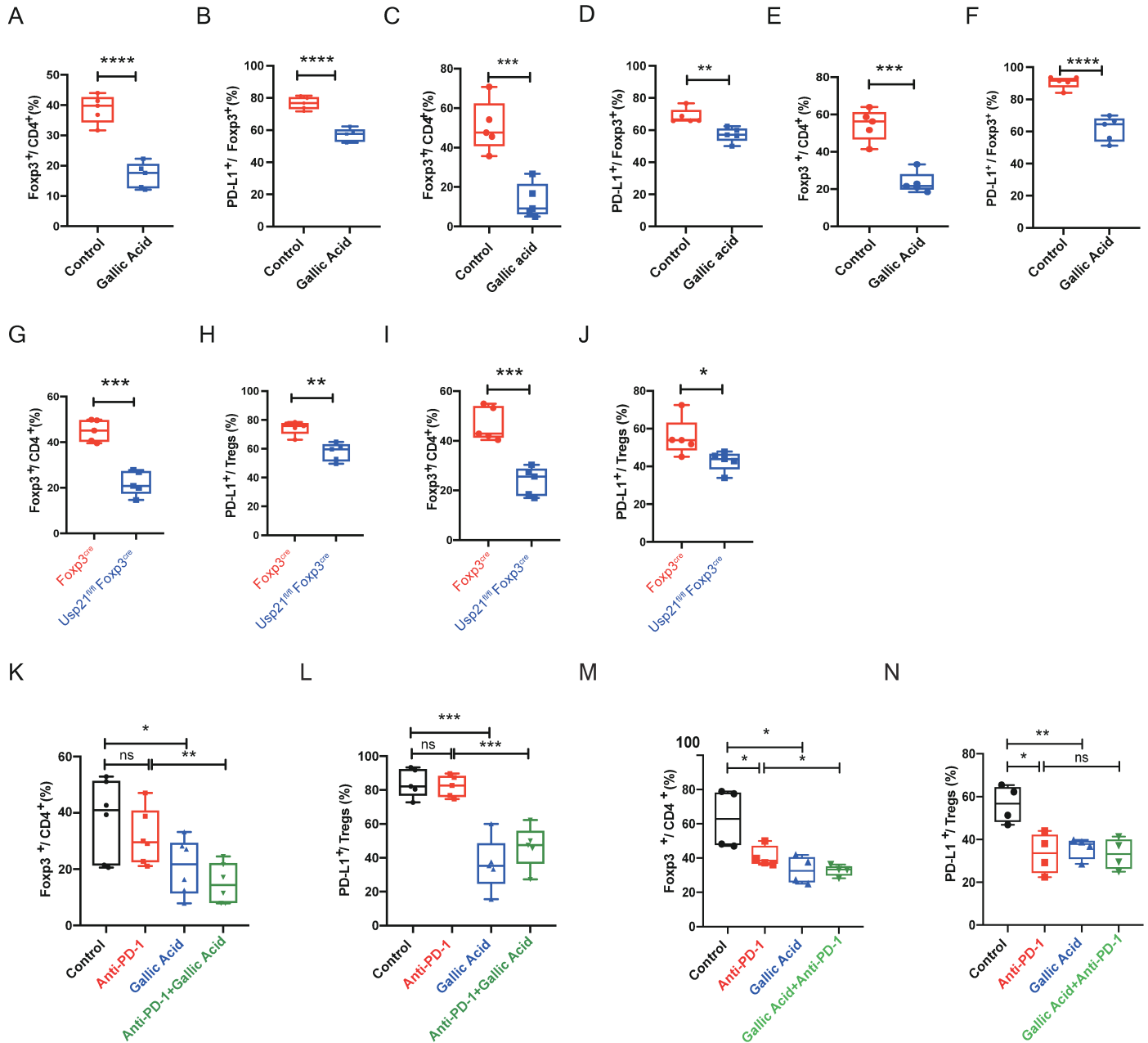


## Supplementary figure 2

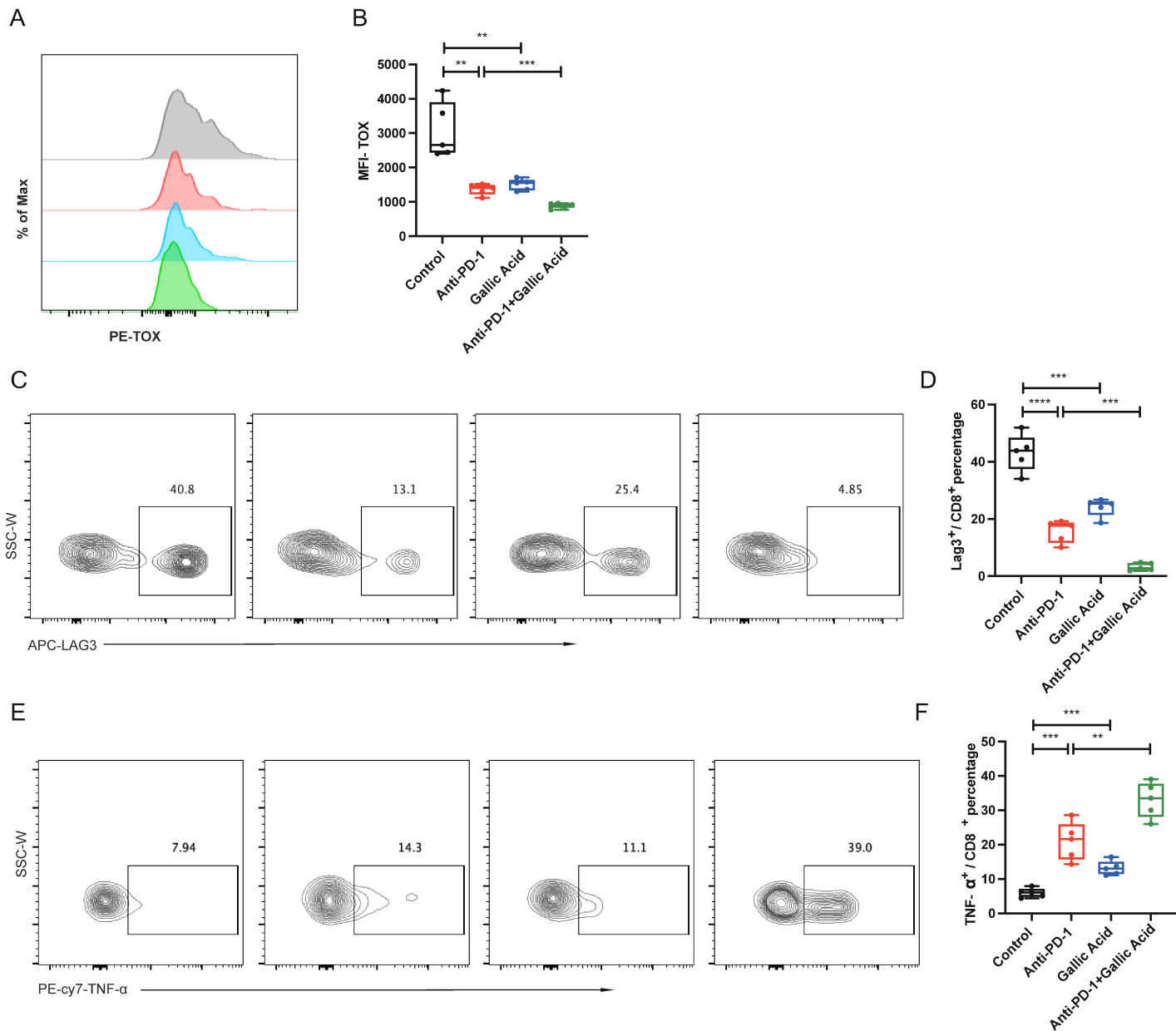




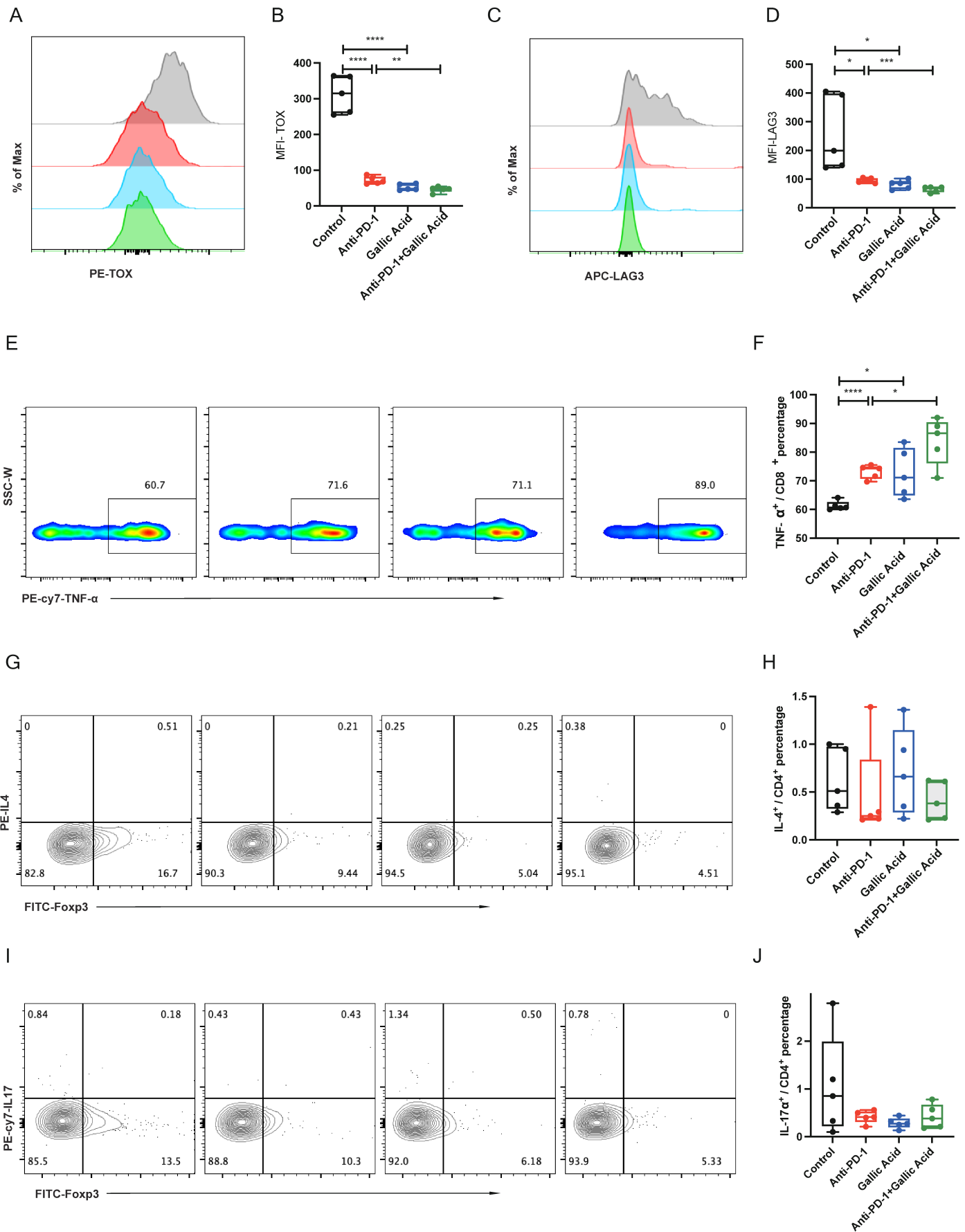
## Supplementary figure 4



## Supplementary figure 5



Supplementary figure 6



**Supplementary Table 1 Clinical characteristics of CRC patients**

Gender	Age at diagnostic	Disease features
Female	70	Rectum adenocacinoma
Female	58	Papillary tubular adenocarcinoma
Male	81	Rectum adenocacinoma
Male	57	Tubular adenocarcinoma
Female	72	Tubular adenocarcinoma
Female	72	Rectum adenocacinoma

**Supplementary Table 2 ChIP-qPCR primers**

Gene	Forward (5'-3')	Reverse (5'-3')
<i>Usp21</i> -promoter	TCCCATGCTCATGTTCTCTTGC	GGCCCAGTCCTAGGAGAGATGTT

**Supplementary Table 3 qRT-PCR primers**

Gene	Forward (5'-3')	Reverse (5'-3')
<i>Usp21</i>	TGATGACTGAGCCAACCACC	CGTCCCAGCTCCAGTTTCTT
<i>Foxp3</i>	TCCTATCCCCTCCCCTGACAC	GCCTTGGTCAGTGCCATTTTC
<i>CD274</i>	ATTTGCTGAACGCCCCATAC	TTGGTGGTGGTGGTCTTACC
<i>Mdm2</i>	GGTGGGAGTGATCAAAGGA	ACACAGAGCCAGGCTTTCAT
<i>Stub1</i>	TACCTCTCCAGGCTCATTGC	TCTTGCCACACAGGTAGTCG
<i>Cblb</i>	CTGACAGGCAGAACTCACCA	AGACTTTGGTGAACCCGTTG
<i>Rnf31</i>	GTCGGAGCTGTGAGGACTTC	TCACCCTGCAGTTAGGCTCT
<i>Usp7</i>	GGAAGCGGGAGATACAGATGA	AAGGACCGACTCACTCAGTCT
<i>Usp44</i>	CTCAACCCTCAGAAATGGCAC	ACGTCGTAGTAACTTCAGGTCTC
<i>Usp22</i>	TGGAAATAATCGCCAAGGAG	GAAGCATGTGTTCCCAAGGT

**Supplementary Table 4 Summary of 31 small molecules down regulating FOXP3**

Names	Code
Procyanidin B2	A1-007
Chelerythrine	A1-106
Gallic acid	B1-061
Sinomenine	C1-053
Corynoxine	E1-012
Caffeic acid	E1-013

Liquiritigenin	E1-072
Palmitic acid	F1-001
Ginsenoside Rb2	H-011
Galantamine Hydrobromide	H-064
gallic acid ethanol ester	H-085
Benzalkonium chloride	J102
Sodium nitroferricyanide dihydrate	J140
Deferoxamine mesylate salt	J505
Daunorubicin hydrochloride	J403
(2,2-Dichloro-1,1-difluoroethyl) methyl ether	J312
(+)-Usniacin (D-Usnic acid)	L1700-07-A10
Limonin	L1700-15-E6
Ramelteon (TAK-375)	L1700-02-H8
Estrone	L1700-05-C2
Niacin (Nicotinic acid)	L1700-05-G8
Tiotropium Bromide hydrate	L1700-10-A5
Tizanidine HCl	L1700-13-C10
Cyclophosphamide monohydrate	L1700-14-H4
DL-Adrenaline	L1700-15-G2
Nicorandil (Ikorel)	L1700-06-F2
Bleomycin sulfate	L1700-02-E10
Fluconazole	L1700-03-C7
Ibutilide Fumarate	L2000-01-B7
Ticagrelor	L2000-03-G3
Bismuth Subcitrate Potassium	L2000-03-D5